



UNIVERSITY OF LEEDS

This is a repository copy of *Review of groundwater flow and contaminant transport modelling approaches for the Sherwood Sandstone aquifer, UK; insights from analogous successions worldwide*.

White Rose Research Online URL for this paper:

<https://eprints.whiterose.ac.uk/186690/>

Version: Accepted Version

---

**Article:**

Medici, G and West, LJ [orcid.org/0000-0002-3441-0433](https://orcid.org/0000-0002-3441-0433) (2022) Review of groundwater flow and contaminant transport modelling approaches for the Sherwood Sandstone aquifer, UK; insights from analogous successions worldwide. *Quarterly Journal of Engineering Geology and Hydrogeology*, 55 (4). qjegh2021. ISSN 1470-9236

<https://doi.org/10.1144/qjegh2021-176>

---

© 2022 The Author(s). Published by The Geological Society of London. All rights reserved. This is an author produced version of an article published in *Quarterly Journal of Engineering Geology and Hydrogeology*. Uploaded in accordance with the publisher's self-archiving policy.

**Reuse**

Items deposited in White Rose Research Online are protected by copyright, with all rights reserved unless indicated otherwise. They may be downloaded and/or printed for private study, or other acts as permitted by national copyright laws. The publisher or other rights holders may allow further reproduction and re-use of the full text version. This is indicated by the licence information on the White Rose Research Online record for the item.

**Takedown**

If you consider content in White Rose Research Online to be in breach of UK law, please notify us by emailing [eprints@whiterose.ac.uk](mailto:eprints@whiterose.ac.uk) including the URL of the record and the reason for the withdrawal request.



[eprints@whiterose.ac.uk](mailto:eprints@whiterose.ac.uk)  
<https://eprints.whiterose.ac.uk/>

1 **Review of groundwater flow and contaminant transport modelling approaches for**  
2 **the Sherwood Sandstone Aquifer, UK; insights from analogous successions**  
3 **worldwide**

4

5 Medici G. <sup>1\*</sup>, West LJ<sup>2</sup>

6 <sup>1</sup> Morwick G360 Groundwater Research Institute, College of Engineering and Physical  
7 Science, University of Guelph, Guelph, Ontario, N1G2W1

8 <sup>2</sup> School of Earth and Environment, University of Leeds, Woodhouse Lane, Leeds, W  
9 Yorkshire LS2 9JT, UK

10 \* Correspondence: [giacomo.medici@g360group.org](mailto:giacomo.medici@g360group.org)

11

12 **Abstract**

13 Sandstones are characterized by different hydraulic behaviours and need to be modelled  
14 in various ways to represent groundwater flow and contaminant transport. This review  
15 shows how sandstone aquifers within the UK Triassic Sherwood Sandstone Group, can be  
16 represented using three modelling approaches; the Conduit Network, Discrete Fracture  
17 Network and Equivalent Porous Medium.

18 The Sherwood Sandstone Aquifer is dominated by matrix flow in the Eastern England  
19 Shelf, Worcester, Needwood and Staffordshire basins. Here, the aquifers are modelled as  
20 Equivalent Porous Media at a range of scales. Fractures represent the principal flow  
21 pathways in the Cheshire Basin. Here, Discrete Fracture Network models that account for  
22 diffusivity in the matrix can be used where the scale of the model domain is small. The  
23 Sherwood Sandstone aquifer across north-western England shows evidence of intense

24 groundwater alteration and high flow velocities in conduits. Turbulent flowing pipe-  
25 elements can be inserted in the modelling domain represented by Equivalent Porous  
26 Medium at specific sites. The review shows how the Sherwood Sandstone Aquifer as well  
27 as other siliciclastic deposits across the world need to be represented using a range of  
28 modelling approaches, as they behave as matrix or fracture flow aquifers, or in specific  
29 cases show a karst-like behaviour.

30

31 **Keywords:** Flow modelling, Sherwood Sandstone Aquifer, Scale, Fracture, Porosity,  
32 Conduit

33

### 34 **Introduction**

35 Contaminants are transported at different rates in sandstone aquifers at relatively shallow  
36 depths depending on the proportion of intergranular to fracture permeability (Gogu et al.  
37 2003; Powell et al. 2003). Indeed, hard sandstones tend to be heavily fractured and  
38 characterized by low values of effective porosity and hence relatively high groundwater  
39 flow velocities occur and large well-head protection areas are designed around abstraction  
40 wells (Freeze and Cherry 1976; Cook 2003; Offerdinger et al. 2019; Troeger and Chambel  
41 2021). Such sandstone-types can also be characterized by karst-like conduits, due to  
42 dissolution of primary and secondary calcite, dolomite and aragonite. These carbonate  
43 minerals precipitated and sealed fractures and adjacent pores before subsequent  
44 dissolution as a consequence of lithospheric uplifts and exposures to freshwater circulation  
45 (Burley 1984; Barker et al. 1998; Kůrková et al. 2019; Meus and Willems 2021). This  
46 telogenetic process coupled with elevated flow velocities allows for genesis of cavities by  
47 also dissolving feldspathic grains, and occurrence of turbulent flow in sandstones of fluvio-  
48 aeolian origin (Burley 1984; Kůrková et al. 2019). Conversely, porous and poorly fractured

49 sandstones are characterized by laminar flow and slow dispersal of pollutant species in  
50 groundwater at relatively slow rates (Worthington 1977; Tellam and Barker 2006).

51 To face this hydraulic complexity, hydrogeologists need to consider that to model  
52 groundwater flow in a porous and fractured sandstone, three alternative modelling  
53 approaches might be necessary as function of modelling objective, observation scale and  
54 proportions between intergranular and fracture permeabilities: Equivalent Porous Medium  
55 (EPM), Discrete Fracture (DFN) and Conduit (CN) network approaches (Barker et al.  
56 1998; Selroos et al. 2002). From a computational standpoint, the simplest flow modelling  
57 approach is EPM where the flow velocities exclusively depend on the hydraulic gradient,  
58 the bulk hydraulic conductivity and the effective porosity. This method treats a sandstone  
59 using bulk properties rather than the physical characteristics of the intergranular pores,  
60 platy fractures and conduits of approximately pipe-shape (Selroos et al. 2002). By  
61 contrast, DFN and CN approaches represent groundwater flow in individual fractures and  
62 channels, respectively (Shoemaker et al. 2008; Hill et al. 2010; Gallegos et al. 2013;  
63 Parker et al. 2019; Medici et al. 2021). These approaches to modelling groundwater flow  
64 and contaminant transport were recently reviewed by Medici et al. (2021) with respect to  
65 the carbonate aquifers of Great Britain and North America. In contrast, in this review, we  
66 focus our attention on modelling groundwater flow in a sandstone aquifer of fluvio-aeolian  
67 origin, the Triassic Sherwood Sandstone Aquifer of Great Britain, which shows a spectrum  
68 of hydraulic behaviours across the country (Allen et al. 1997; Tellam and Barker 2006;  
69 Medici et al. 2019a, b).

70 The Sherwood Sandstone Aquifer (Figs. 1, 2) is particularly suitable for studying the  
71 different approaches to groundwater flow modelling in siliciclastic aquifers for two reasons.  
72 Firstly, calcite, aragonite and dolomite represent the principal minerals that fill bedding  
73 discontinuities and fractures in this sandstone of Triassic age (Burley 1984; Strong et al.  
74 1994; Medici et al. 2018). These minerals are highly soluble in groundwater and can

75 dissolve, resulting in the formation of karst-like conduits. Together with pores and  
76 fractures, such conduits represent further hydraulic elements to be inserted in a model  
77 domain. Secondly, a diverse suite of background hydrogeological materials (e.g., core plug  
78 porosity and permeability tests, fluid logging, tracer tests and groundwater flow models) is  
79 available on the Sherwood Sandstone Aquifer since it represents the second most  
80 important UK aquifer in terms of volume of abstraction (Harris and Lowe 1984; Allen et al.  
81 1997; Smedley and Edmunds 2002; Goody et al. 2005; Streetly et al. 2000, 2006; Rivett  
82 et al. 2007; Abesser and Lewis 2015), and it serves as the bedrock lithology of large  
83 industrial cities such as Birmingham, Liverpool, Nottingham and Manchester (Waltham  
84 1993; Ford and Tellam 1994; Tellam 1995; Allen et al. 1997, 1998; Bottrell et al. 2008;  
85 Banks et al. 2013; Colyer et al. 2021). Hence, establishing a link between the hydraulic  
86 behaviour of the Sherwood Sandstone Aquifer and appropriate modelling techniques is  
87 achievable.

88 Large availability of background data on the hydrogeology of the Sherwood Sandstone  
89 Aquifer has prompted other review papers in the last thirty years. A collection of  
90 permeability tests on core plugs, pumping tests and tracer tests on the Sherwood  
91 Sandstone Aquifer can be found in Allen et al. (1997). Further hydraulic data were  
92 acquired on the Sherwood Sandstone Aquifer to characterize the aquifer properties at a  
93 variety of scales (e.g., Rivers et al. 1996; Hitchmough et al. 2007; Bashar and Tellam  
94 2011; Medici et al. 2016, 2018). New advances were made by numerous authors in  
95 understanding the three dimensional fracturing pattern that controls groundwater flow in  
96 the Sherwood Sandstone Aquifer of Great Britain (e.g., Allen et al. 1998; Gutmanis et al.  
97 1998; Wealthall et al. 2001).

98 Tellam and Barker (2006) reviewed the physical and chemical properties of the Sherwood  
99 Sandstone Aquifer in detail, but without incorporating groundwater flow models. A recent  
100 review analysed the existing background information to extract useful hydraulic information

101 for the analogue Triassic successions that host hydrocarbon resources off-shore (Medici et  
102 al. 2019a). However, Medici et al. (2019b) studied the ratio between the hydraulic  
103 conductivity at the scale of the pumping test ( $K_{\text{well-test}}$ ) and the core plug ( $K_{\text{core-plug}}$ ) that  
104 regionally varies across the Sherwood Sandstone Aquifer in Great Britain. This ratio ( $K_{\text{well-}}$   
105  $\text{test}/K_{\text{core-plug}}$ ) appears sensitive to the sedimentary basin in the country (see locations of  
106 grabens in Figures 1a, b) and is diagnostic to define the hydraulic behaviour of the aquifer  
107 and variation in permeability with scale (Allen et al. 1997; Medici et al. 2019a, b). Hence,  
108 the above mentioned ratio represents a starting point for this review. Details on the  
109 influence of mechanical strength and style of deformation on permeability type (i.e.,  
110 fracture versus matrix flow) of the Sherwood Sandstone Group across the UK basins were  
111 also recently reviewed (Medici et al. 2019b). In contrast with previous reviews on the  
112 hydrogeology of Sherwood Sandstone Aquifer, the physical properties of the aquifer are  
113 here reviewed focussing on groundwater flow modelling. The review aims to relate the  
114 different hydraulic behaviours of the Sherwood Sandstone Aquifer to the three different  
115 approaches to difference and finite element modelling (see Fig. 3) used to model  
116 groundwater flow in porous and fractured rocks. The review focuses on the initial choice of  
117 the modelling approach to groundwater and contaminant transport representation based  
118 on the purpose and scale of the project, and the hydraulic properties of the sandstone. In  
119 terms of modelling purpose, we distinguish between simulations that only need to predict  
120 bulk water movement (e.g., for water resource assessment), and those that require  
121 groundwater velocity simulation (e.g., for reactive transport modelling of pollutant  
122 migration). Note that parameters required for reactive contaminant transport modelling of  
123 specific pollutants were not considered in this review.

124 Specific objectives are as follows: (i) identify the principal hydro-mechanical features of the  
125 aquifer across the country, (ii) review previous groundwater flow and contaminant

126 transport modelling studies, and (iii) address future modelling research needs in the  
127 Sherwood Sandstone Aquifer through comparisons with similar aquifers overseas.

128

129

130

131

## 132 **Geological background**

### 133 *Basin evolution and stratigraphy*

134 The Triassic Sherwood Sandstone Group comprises a continental sedimentary succession  
135 of fluvial and aeolian deposits accumulated in a series of sedimentary basins. Such  
136 geological basins developed as a consequence of the break-up of the Pangaea  
137 supercontinent during the Permo-Triassic and host the sedimentary succession studied in  
138 this research (Mountney and Thompson 2002; Brookfield 2008; McKie and Williams 2009;  
139 Medici et al. 2015; Newell 2018). Fluvial deposits were related to the major braided fluvial  
140 system that filled the rift basins of Great Britain under semi-arid to arid climate conditions  
141 (Thompson 1970; Schmid et al. 2006).

142 Extensional tectonics characterized NW Europe after the Permo-Triassic time throughout  
143 the Jurassic and Cretaceous (Chadwick and Evans 1995). After this time, NW Europe was  
144 uplifted during the Cenozoic Era (Carminati et al. 2009; Kortas and Younger 2013). This  
145 lithospheric uplift is considered responsible for the development of high-angle (70° – 90°)  
146 inclined stratabound joints (*sensu* Odling et al. 1999) which terminate in correspondence  
147 of fractures at very low angle (0° – 15°) relative to bedding (Gutmanis et al. 1997; Odling et  
148 al. 1999). The Sherwood Sandstone Group has also been affected by deep mining of  
149 underlying Carboniferous Coal Measures in the coalfields on Nottinghamshire,  
150 Staffordshire and Yorkshire that has resulted in coal working collapse and fracturing in the  
151 lower parts of the overlying strata (Allen et al. 1998; Barker and Tellam 2006). The

152 sediments that formed the Sherwood Sandstone Aquifer filled a series of sedimentary  
153 basins in Great Britain which are illustrated in Figure 1b. The Wessex, Worcester,  
154 Staffordshire, Needwood, Cheshire, Eastern Irish Sea and Vale of Eden basins are all at  
155 least partially bounded by palaeo-rift faults. However, the Eastern England Shelf is a shelf-  
156 edge type basin not-bounded by faults and therefore it represents an exception in the  
157 Triassic realm of Great Britain.

158 In all the above mentioned Triassic basins, the basal part of the Sherwood Sandstone  
159 Group is dominated by fluvial deposits, which are primarily characterized by channel-fill  
160 architectural elements (Fig. 2, Ambrose et al. 2014). The fluvial palaeocurrent direction is  
161 towards the north due to the principal sediment source which is represented by the  
162 Armorican Massif in northern France (Newell 2018; Figs. 1a, 2). Northward decrease in  
163 mean grain-size and maximum clast-size characterizes the fluvial deposits of the  
164 Sherwood Sandstone Group as a consequence of the increasing distance from the fluvial  
165 sediment source (Fig. 2; Smith 1990; McKie and Williams 2009). Fluvial deposits of Lower  
166 Triassic age range from conglomerates (LA1 Lithofacies Association 1, Fig. 4a, b) in the  
167 Wessex, Worcester, Staffordshire, Needwood, Cheshire and southern parts of the Eastern  
168 England Shelf basins, to fine-grained sandstone in the northern part of the Eastern  
169 England Shelf, Eastern Irish Sea Basin, Vale of Eden and Carlisle basins (Fig. 4 c, d;  
170 Mickie and Williams 2009; Ambrose et al. 2014; Medici et al. 2019b). The Sherwood  
171 Sandstone Group shows an upward trend from conglomerates (LA1) via feldspathic  
172 sandstone of fluvial origin (LA2), into sand-prone and quartz-rich deposits which are  
173 characterized by facies of exclusively aeolian origin (LA3 Lithofacies Association 3, Figs.  
174 2, 4c, 5a, b).

175 Fluvial lithofacies associations are characterized by conglomerate and pebbly sandstone  
176 lithofacies (LA1), and sandstone channels interbedded with floodplain mudstone (LA2).  
177 However, lithofacies associations of aeolian origin (LA3) are dominated by cross-bedded



178 dune deposits. Fine grained sandstones related to damp interdune and mudstone of wet  
179 interdune and mudstone wet interdune origin also characterize the aeolian deposits (LA 3)  
180 of the Sherwood Sandstone Group. Note that, reference to these three facies associations  
181 (LA 1-3) is crucial in this manuscript to establish a link between lithology, mechanical  
182 behaviour and flow modelling approach.

183

184

### 185 *Structural style and mechanical behaviour of the stratigraphic units*

186 Development of stratabound and non-stratabound joints and bedding plane fractures is  
187 highly determined by lithology and mechanical properties in the Sherwood Sandstone  
188 Aquifer. The bedding plane fractures in the Eastern Irish Sea Basin (Figure 4c) are  
189 characterized by lateral continuities up to 300 m (Medici et al. 2015). Stratabound and  
190 bedding plane discontinuities reactivated by tectonic stresses are particularly well  
191 developed in the relatively brittle, highly mechanically resistant (17-36 MPa of uniaxial  
192 compressive strength under natural saturation conditions,  $UCS_{nat}$ ) Sherwood Sandstone  
193 Aquifer of the Eastern Irish Sea and Cheshire basins (Fig. 4c, 5a, 6a-c; Allen et al. 1998;  
194 Hitchmough et al. 2007). Here, high angle joints have been found partially filled by clays in  
195 the vadose zone in the Runcorn Peninsula (Wealthall et al. 2001). By contrast, sub-vertical  
196 joints are more widely spaced and non-stratabound in the Eastern England Shelf. This  
197 structural pattern arises from the relatively ductile, low mechanical resistance ( $UCS_{nat} < 20$   
198 MPa; Yates 1992) of the Sherwood Sandstone Group in the shelf-edge basin of England  
199 as illustrated in the conceptual scheme in Figure 7. Stratabound joints are exclusively  
200 present in the 1-2 m thick sandstone layers interbedded with conglomerates (LA1  
201 lithofacies association) in the Kidderminster Sandstone Formation (Figure 7 upper panel)  
202 of the Worcester, Needwood and Staffordshire basins. Notably, the low-mechanical  
203 resistance ( $UCS_{nat} < 16$  MPa; Whitaker and Turner 1989) of the conglomerates also in the

204 latter case impedes development of stratabound fractures. Scanline surveys of rock  
205 discontinuities undertaken at road cuts in the Helsby and Wildemoor Sandstone formations  
206 show higher fracturing density in the fluvial deposits (which are less porous and more  
207 mechanically resistant) than in the aeolian deposits (Fig. 7 middle and lower panels; Allen  
208 et al. 1997, 1998). The fluvial channels (LA2 Lithofacies Association) and aeolian dunes  
209 (LA3 Lithofacies Association) are characterized by an average lateral spacing of sub-  
210 vertical joints of 2.0 and 3.1 meters, respectively (Allen et al. 1998; Wealthall et al. 2001;  
211 Hitchmough et al. 2007).

212 Fault zones in aeolian dunes are also characterized by development of low permeability  
213 deformation bands rather than open fractures, as seen in fluvial sequences worldwide  
214 (Aydin 2000; Bense et al. 2013). Extensional faults are highly permeable in the fluvial St  
215 Bees Sandstone of west Cumbria and dilatational jogs enlarged by groundwater flow and  
216 cavities are recognized in outcrop (Fig. 5c). Boreholes collapse in correspondence of such  
217 tectonic structures, cavities with apertures in the range 0.05 - 0.6 m large are recognized  
218 by optical televiewer logs in correspondence of bedding plane fractures (Fig. 6a, b), and  
219 calcite dissolves in sub-vertical joints (Fig. 6c) in the Sherwood Sandstone Aquifer of west  
220 Cumbria (Medici et al. 2016). Further details on the hydro-structural pattern of fault zones  
221 and development of extensional features in fluvial and aeolian deposits can be found in  
222 Medici et al. (2019b).

223

## 224 **Physical Hydrogeology**

### 225 *Core plug and well-test scale properties*

226 Intergranular hydraulic conductivities measured using the Darcy's law on core plugs vary  
227 within eight orders of magnitude from  $1.2 \times 10^{-11}$  to  $1.0 \times 10^{-4}$  m/s in the Sherwood  
228 Sandstone Aquifer (Allen et al. 1997). This high variability is related to heterogeneities

229 (e.g., mudstone) that characterize the three distinct lithofacies associations (LA1-3), as  
230 illustrated in Figures 4, 5 and 7.

231 Intergranular hydraulic conductivities are only slightly reduced (by 6-20 %) in response to  
232 an increase in lithostatic pressure of 7 MPa (overburden pressure of 300 m below the  
233 subsurface) as tested at the core-plug scale by Daw et al. (1974). In contrast, fracture flow  
234 is strongly reduced (by 65-80%) in experiments that applied the same amount of  
235 overburden pressure (7 MPa) to plugs with a single discontinuity (Daw et al. 1974). The  
236 aquifer is highly anisotropic and the ratio between horizontal ( $K_h$ ) and vertical hydraulic  
237 conductivity ( $K_v$ ) ranges from 1.5 to 100 and 2 to 34 at the core plug and well test scale,  
238 respectively (Allen et al. 1997; Streetly et al. 2000; Pokar et al. 2006; Medici et al. 2018).

239 Transmissivities in the Sherwood Sandstone Aquifer show similar values across the  
240 regions of Great Britain, i.e. median values range from  $1.6 \times 10^{-3}$  m<sup>2</sup>/s to  $3.5 \times 10^{-5}$  m<sup>2</sup>/s in  
241 the various Permo-Triassic basins (Brassington and Walthall 1985; Allen et al. 1997, 1998;  
242 Tellam and Barker 2006; Medici et al. 2019a). Such transmissivity values show a positive  
243 correlation with the well-screen length (Allen et al. 1997).

244 In contrast to transmissivity values, the ratio ( $K_{\text{well-test}}/K_{\text{core-plug}}$ ) between hydraulic  
245 conductivity values from pumping tests and core plugs shows a regional distribution across  
246 the Triassic basins of Great Britain. Notably, the hydraulic conductivity from pumping tests  
247 is  $\sim 10^2$  times higher than that derived testing core-plugs collected from the Eastern Irish  
248 Sea Basin of west Cumbria at shallow depths ( $< \sim 150$  mBGL; Allen et al. 1997; Streetly et  
249 al. 2000). Here, pumping tests show the highest transmissivity value,  $1.0 \times 10^{-2}$  m/s, in a  
250 valley. This is a hydraulic scenario common to moderately karstified aquifers such as the  
251 Magnesian Limestone and the Chalk in England (Allen et al. 1997; Worthington and Ford  
252 2009), suggesting that the sandstone here is locally characterized by a karst-like  
253 behaviour. The ratio between well-test derived hydraulic conductivity and those from core  
254 plugs measured by mini-permeameters is  $\sim 5$  in the Sherwood Sandstone Aquifer in the

255 Cheshire Basin. This value is the result of a pervasive fracture network due to the high  
256 mechanical resistance ( $UCS_{nat} = 30$  MPa) combined with a relatively low hydraulic  
257 conductivity matrix (Brassington and Walthall 1985; Hitchmough et al. 2007). The area of  
258 the Sherwood Sandstone Aquifer that shows the lowest difference between well-test and  
259 core-plug hydraulic conductivities ( $< 2.0$ ) is the Eastern England Shelf and Worcester  
260 Basin (Allen et al. 1997; Ramingwong 1974). This hydraulic scenario arises from low  
261 values of mechanical resistance ( $UCS_{nat} < 20$  MPa) that impedes development of a  
262 pervasive fracturing network in the latter two Triassic basins (Whitworth and Turner 1989;  
263 Yates 1992); the aquifers developed in these basins are thus mainly dominated by  
264 intergranular flow.

265

#### 266 *Fluid logging*

267 Bedding plane discontinuities, sub-vertical joints and extensional faults are all capable of  
268 facilitating flow in the Triassic Sherwood Sandstone Aquifer (Tellam and Barker 2006;  
269 Medici et al. 2016). In fact, bedding plane fractures were detected as pathways at shallow  
270 depths ( $< 150$  mBGL) by borehole fluid electrical conductivity and temperature logging  
271 under natural conditions in the Eastern Irish Sea Basin (Medici et al. 2016, 2018),  
272 Cheshire (Hitchmough et al. 2007), Worcester (Allen et al. 1998) basins and the Eastern  
273 England Shelf (Rivers et al. 1996). In the Eastern Irish Sea Basin, high angle ( $70^\circ - 90^\circ$ )  
274 inclined stratabound joints also provide occasional support to flow at their intersection with  
275 bedding plane fractures in the shallow ( $< 100$  mBGL) Sherwood Sandstone Aquifer (Medici  
276 et al. 2016, 2018).

277 This hydraulic scenario was characterised by borehole flow logging under natural condition  
278 in the highly mechanically resistant ( $UCS_{nat} = 17-36$  MPa) St Bees Sandstone aquifer of  
279 the Eastern Irish Sea and Cheshire basins (Medici et al. 2016; Hitchmough et al. 2007).  
280 Fluid temperature and electrical conductivity logs were also undertaken in the Sherwood

281 Sandstone Aquifer in the Vale of York (Allen et al. 1998) and Nottinghamshire (Rivers et  
282 al. 1996). Here, inflows from fissures were detected only in the first 10 meters below the  
283 water table due to greater dissolution in the shallow part of the aquifer zone. Below this  
284 threshold, the aquifer behaved as a matrix flow aquifer and variation in fluid temperature  
285 and electrical conductivity were absent in the Vale of York and Nottinghamshire.

286 Quantitative flow logging analysis was performed using the Flow Log Analysis Single Hole  
287 (FLASH, Day-Lewis et al. 2011) program in the St Bees Sandstone of west Cumbria. Here,  
288 the latter methodology developed by the United States Geological Survey (USGS) to  
289 compute profiles of hydraulic conductivity has been applied due to the availability of both  
290 fluid velocity logs and pumping tests (Medici et al. 2016). Notably, the use of the USGS  
291 FLASH program failed on three boreholes matching experimental and modelled fluid flow  
292 velocities in wells characterized by sharp variation of velocities in correspondence of  
293 conduits 5-10 cm in diameter (Medici et al. 2016). This scenario can arise from turbulent  
294 flow occurring in correspondence of such conduits enlarged by dissolution of the high-  
295 solubility cement (Day-Lewis et al. 2011; Medici et al. 2016).

296

### 297 *Tracer testing*

298 Very few successful field-scale point-to-point tracer tests have been carried out in the  
299 Sherwood Sandstone Aquifer due to the simplistic assumption that the sandstone is  
300 primarily a matrix flow aquifer across all the Great Britain (Allen et al. 1997, 1998; Barker  
301 et al. 1998; Streetly et al. 2002; Tellam and Barker 2006; Riley et al. 2011). Tracer  
302 movement was considered slow by hydrogeologists and high dilution a problem that might  
303 prevent detection at field-site scale (Allen et al. 1998).

304 However, results from a few point-to-point tracer tests are available in the Sherwood  
305 Sandstone Aquifer of the Yorkshire, West Midlands and Cheshire regions. Low travel  
306 times of  $1.7 \times 10^{-5}$  and  $3.5 \times 10^{-5}$  m/s, perhaps indicating matrix flow, characterize this

307 sandstone aquifer at Carlton in the Eastern England Shelf and Hodnet in the Worcester  
308 Basin, respectively (Allen et al. 1997, 1998). Hydrogeologists injected fluorescent dye into  
309 an observation borehole and recorded the breakthrough at inflows along a tunnel in  
310 Liverpool in the Cheshire Basin (Barker et al. 1998; Streetly et al. 2002). Here, the average  
311 linear flow velocity was  $1.6 \times 10^{-3}$  m/s which more typically can be found in karst aquifers of  
312 carbonate origin instead of porous sandstone (Hartmann et al. 2014; Worthington 2015).

313 In summary, the physical hydrogeology of Sherwood Sandstone Aquifer shows a range of  
314 scale effects depending on the important of matrix versus fracture or conduit flow. In  
315 Sherwood Sandstone Aquifer where matrix flow dominates, it is likely that a  
316 Representative Elementary Volume (REV, *sensu* Schulze-Makuch et al. 1999; Schulze-  
317 Makuch 2005) can be defined at the approximately 10m scale. In these cases, the  
318 hydraulic conductivity above that scale becomes constant and tracer testing is not  
319 necessary. Where fracture flow dominates, it may also be the case that REV can be  
320 defined at such a scale, taking into account that the spacing of bedding plane fractures  
321 and joints is smaller than 10m, provided that the effect of large faults is taken into account  
322 separately, where these occur on the 100m – 1km scale (Medici et al. 2016; Bense et al.  
323 2013). However, where karst-like conduits are present, no REV can be defined (Schulze-  
324 Makuch et al. 1999; Hartman et al. 2014; Medici and West 2021). In such cases, the  
325 hydraulic conductivity will continue to increase with scale, up to the characteristic length of  
326 the connected conduits that can be detected by tracer testing.

327

## 328 **Groundwater Flow Modelling**

### 329 *Previous models*

330 Groundwater flow models in the shallow (< 120 mBGL) Sherwood Sandstone Aquifer were  
331 developed in most cases using the EPM as the modelling approach and MODFLOW as  
332 the numerical code, respectively (see type of approach, location and numerical code used

333 for flow models in Table 1). MODFLOW groundwater flow models at a relatively large (~  
334 200 km<sup>2</sup>) scale were developed in the Eastern England Shelf to constrain aquifer recharge  
335 and designate capture zones around areas of abstraction in both the Vale of York (Bottrell  
336 et al. 2006) and Nottinghamshire using MODFLOW/MODPATH to trace unreactive  
337 particles (Tab.1; Bishop and Ruston 1993; Allen et al. 1997; Zhang and Hiscock 2010).  
338 However, exclusively in Nottinghamshire, MODFLOW-MT3DMS large-scale contaminant  
339 transport models are publicly available that represent plume development in the  
340 subsurface and predict nitrate concentrations in supply wells (Davison and Lerner 2000;  
341 Zhang and Hiscock 2011, 2016). All the above mentioned groundwater flow models were  
342 calibrated using horizontal hydraulic conductivity ( $1.2 \times 10^{-6}$  -  $6.9 \times 10^{-5}$  m/s) values that are  
343 within the range of the values derived from core plugs and pumping tests in the Sherwood  
344 Sandstone Aquifer of the Eastern England Shelf (Bishop and Ruston 1993; Davison and  
345 Lerner 2000; Neumann and Hughes 2003; Bottrell et al. 2006; Pokar et al. 2006; Zhang  
346 and Hiscock 2010, 2011). Note that matching the hydraulic conductivity values of the core-  
347 plug with those of the regional scale is common for aquifers largely dominated by  
348 intergranular flow and characterized by a small REV (*sensu* Schulze-Makuch et al. 1999;  
349 Schulze-Makuch 2005).

350 The Sherwood Sandstone Aquifer was treated as a single hydraulic unit in groundwater  
351 flow models developed for the Eastern England Shelf (Bishop and Ruston 1993; Davison  
352 and Lerner 2000; Neumann and Hughes 2003; Bottrell et al. 2006; Zhang and Hiscock  
353 2010, 2011). In this sedimentary basin, the latter choice is reasonable given the relative  
354 homogeneity of the sandstone and the fact that the British Geological Survey could not  
355 recognize stratigraphic members in quarries and core logs (Ambrose et al. 2014;  
356 Wakefield et al. 2015). The Sherwood Sandstone Aquifer was also modelled as a single-  
357 layer in the MODFLOW-EPM model developed in the Birmingham area of the Worcester  
358 Basin (Knipe et al. 1993; Rivett et al. 2012). Here, the Bromsgrove, Wildmore and

359 Kidderminster Sandstone formations were treated as a single unit with a hydraulic  
360 conductivity of  $1.7 \times 10^{-5}$  m/s and an effective porosity of 0.25. This assumption  
361 overlooks the fact that the aeolian facies of the Bromsgrove Sandstone Formation is more  
362 porous and has fewer connective fractures than the fluvial units of the Wildmore and  
363 Kidderminster Sandstone formations (see contrast of fracture density in fluvial vs. aeolian  
364 lithofacies associations in Figure 7). Thus, the Bromsgrove Formation is likely  
365 characterized by higher values of effective porosity (typically set up to around 0.15-0.25 in  
366 particle tracking modelling) and therefore ideally should be represented as different unit for  
367 particle tracking and solute transport modelling (Allen et al. 1997, 1998; Tellam and Barker  
368 2006; Medici et al. 2019a).

369 The Sherwood Sandstone Aquifer in the Merseyside area of the Cheshire Basin was also  
370 modelled in MODFLOW as a single unit in an EPM. Here, a  $2.3 \times 10^{-5}$  m/s background  
371 horizontal hydraulic conductivity was assigned to the entire aquifer. A reduction of three  
372 orders of magnitude was applied in correspondence of faults to simulate the sharp  
373 changes in hydraulic head moving from the footwall to the hanging wall (Tab. 1; Seymour  
374 et al. 2006). The Sherwood Sandstone Aquifer is anisotropic and the ratio between  
375 horizontal and vertical hydraulic conductivity was defined through calibration in  
376 MODFLOW-EPM models. In such models, the ratio  $K_h/K_v$  is typically tenth-one fitting  
377 values (2-34) from pumping tests in the studied aquifer (Streetly et al. 2000; Zhang and  
378 Hiscock 2010).

379 In contrast to the models described above (see Tab. 1), Hitchmough et al. (2007)  
380 developed a DFN flow model using NAPSAC (by AMEC, Harwell, Oxfordshire; Wilcock  
381 1996) as the numerical code for the Sherwood Sandstone Aquifer in the Cheshire Basin of  
382 the Merseyside area. This research used DFN modelling to assess fracture network  
383 connectivity in its minimum REV of  $35 \times 35 \times 35$  m (Tab. 1). In the latter basin, fractures  
384 are highly conductive ( $K_{\text{well-test}}/K_{\text{core-plug}}=5$ ; Medici et al. 2019b) and a DFN approach at the



385 scale of the industrial field site ( $\sim 10^1 \text{ km}^2$ ) can be used based on a robust characterization  
386 of the fracture network. DFN modelling generates distributions of fractures and bedding  
387 planes and compares these values with observed data from outcrop scanlines and/or  
388 borehole acoustic televiewer logging to represent positions, sizes and mechanical  
389 apertures of those features. To develop the DFN model generated by Hitchmough et al.  
390 (2007), 979 rock discontinuities were characterized performing outcrop scanlines, and  
391 measurements of fracture orientation, aperture, spacing and tortuosities were recorded. In  
392 terms of flow modelling, the latter DFN model of the Sherwood Sandstone Aquifer of the  
393 Merseyside assumes a non-conductive matrix; hydraulic conductivity of bedding plane  
394 discontinuities was extrapolated from packer testing (Hitchmough et al. 2007). Note that  
395 groundwater flow models that incorporate discrete karstic conduits have not been built for  
396 the British Sherwood Sandstone to the authors' knowledge. This scenario might be either  
397 related to absence of a robust characterization that supports the latter modelling solution,  
398 apart from tracer testing in Liverpool (Barker et al. 1998), or an assumption that this  
399 approach is not necessary for the purposes to which their models were developed.

400

#### 401 *Comparisons with other sandstone aquifers*

402 The EPM modelling approach is commonly used in sandstone aquifers for the  
403 management of aquifer water resources across the world (Freeze and Cherry 1976; Hill  
404 and Tiedeman 2006). In this case, EPM modelling is suitable at a variety of scales from  
405 that one of industrial sites ( $< \sim 10 \text{ km}^1$ ) up to the one of a sedimentary basin ( $\sim 10^4 \text{ km}^2$ ) for  
406 sandstone aquifers as depicted on the left side of Figure 8. For example, the EPM using  
407 MIKE-SHE (by DHI Water & Environment, Cambridge, Ontario; Jaber and Shukla, 2012)  
408 as numerical code was used in the Californian Cretaceous Sandstone at the watershed  
409 ( $\sim 15^2 \text{ km}^2$ ) scale in a model that include the vadose zone and the shallowest and highly  
410 permeable saturated zone (Manna et al. 2019). A similar approach to groundwater flow

411 modelling has been used in the Sherwood Sandstone Aquifer to constrain aquifer resource  
412 by model calibration in the shallowest and highly permeable 150 m below the ground  
413 surface (Bottrell et al. 2006). Moving at a smaller (1-5 km<sup>2</sup>) scale to model contaminant  
414 transport the DFN approach was chosen in the Cretaceous sandstones of California and  
415 Colorado and the Cambrian Sandstone of Wisconsin (McKoy and Sams 1997; Pierce et al.  
416 2018; Morgan 2019; Pilato 2021). In the above mentioned case studies, the use of  
417 FRACTRAN and MAFIC (both by Golder Associates, Toronto, Ontario; Miller 1995) as  
418 numerical codes allowed representation of solute advective transport and diffusivity in the  
419 rock discontinuities and matrix (Figure 8 central-right portion of the panel describing  
420 fractured sandstones), respectively. This approach named DFN-M combines EPM and  
421 DFN and can be exported in the Sherwood Sandstone Aquifer where both fractures and  
422 matrix are hydraulically conductive, and diffusivity cannot be neglected (Figure 8 central  
423 portion; Bloomfield and Williams 1995; Bloomfield et al. 2006; Bouch et al. 2006; Tellam  
424 and Barker 2006; Hitchmough et al. 2007).

425 The DFN approach in sandstone aquifers has also been used in the Carboniferous  
426 Sandstone of NE England. This Carboniferous sandstone is highly mechanically resistant  
427 (UCS > 20 MPa) and hydraulic aperture and hence flow velocities are highly sensitive to  
428 stress release in proximity to mineral-pit excavations, i.e. within the so-called excavation  
429 disturbed zone (Foster et al. 2018). This finding was demonstrated via applying a DFN  
430 approach using the ELFEN code (by Rockfield Global, Cardiff, Wales; Rockfield 2001) to  
431 geomechanical modelling by investigating fracture aperture response to stress relaxation  
432 in the Carboniferous Sandstone of Northumberland for a range of excavation profiles. The  
433 mechanical resistance of the Sherwood Sandstone Aquifer is very high (up to 30 MPa) in  
434 north-west England and here similar scenarios can occur with mechanical aperture  
435 increased by stress release within excavations disturbed zones. Indeed, the fracture

436 hydraulic conductivity changes by 65-80% from a 7 MPa normal stress change (Daw et al.  
437 1974).

438 Groundwater flow can enlarge rock discontinuities via dissolution processes in a variety of  
439 rock-types including sandstones. Also, after dissolution of the carbonate cement, silicate  
440 mineral grains can be washed out from fractures in areas characterized by elevated  
441 groundwater flow velocities (Worthington et al. 2016). Note that, the Sherwood Sandstone  
442 Aquifer in west Cumbria where cavities were detected by optical and acoustic televiewer  
443 logs is located in the proximity of the Lake District mountains and hence elevated hydraulic  
444 gradients (0.15-0.35) and intense groundwater flow occur (Black and Brightman 1996;  
445 Medici et al. 2016, 2018, 2019b). Karst-like cavities and caves have been reported in  
446 some other sandstones with calcite cement in five continents; the Devonian in Australia  
447 (Young 1986, 1988), the Carboniferous in Scotland (Balin 2000), the Permian in China  
448 (Yang et al. 2011), the Jurassic in Luxembourg (Meus and Willems 2021), the Cretaceous  
449 in Czech Republic (Kůrková et al. 2019), and the Miocene in Nigeria (Wray 1997). Karst-  
450 like groundwater flow velocities have been found in the Sherwood Sandstone Aquifer in  
451 England ( $1.6 \times 10^{-3}$  m/s average peak flow velocity), the Jurassic Sandstone of Luxembourg  
452 ( $4.4 \times 10^{-3}$  m/s and  $9.7 \times 10^{-2}$  m/s as average pick and maximum flow velocities,  
453 respectively), and the Cretaceous in Czech Republic (maximum flow velocities reported  
454  $2.2 \times 10^{-2}$  –  $2.02 \times 10^{-1}$  m/s) by using tracer testing (Barker et al. 1998; Kůrková et al. 2019;  
455 Meus and Willems 2021). Occurrence of high flow velocities and turbulent flow should not  
456 be discounted in some sandstone aquifers to designate well-head protection areas. For  
457 example, high turbidity was found in the groundwater of the Sherwood Sandstone Aquifer  
458 in the Worcester basin by South Staffs Water (Hudson 2008). Solute transport occurs  
459 through matrix, a network of discrete fractures and a small number of karst-like conduits.  
460 In the latter case, the EPM, DFN and CN needs to be combined to represent this  
461 complexity as shown in the right-lower portion of the panel in Figure 8.

462

463 *Modelling strategy and future research*

464 The shallow (<150 mBGL) Sherwood Sandstone Aquifer is characterized by different  
465 hydraulic behaviours across Great Britain. Hence, the strategy to model groundwater flow  
466 can vary and different approaches may be combined depending on modelling objectives,  
467 observation scale, degree of heterogeneities and nature of permeability as illustrated in  
468 Figure 8. Where modelling is at a relatively large scale (more than 10 km<sup>2</sup> plan area)  
469 representation of individual features such as fractures and conduits may be too  
470 computationally demanding to be feasible. Furthermore, fractures and conduits can lose  
471 connectivity at the basin scale (plan areas ~ 10<sup>2</sup>-10<sup>4</sup> km<sup>2</sup>). In such circumstances,  
472 representation using the EPM approach is likely to represent the only practicable solution,  
473 whatever the modelling objective. This option requires to estimate the equivalent bulk  
474 properties of the modelled layers, for example the EPM hydraulic conductivity, and where  
475 transport is modelled, the effective porosity (Worthington et al. 2012, 2019; Medici and  
476 West 2021; Medici et al. 2021). The EPM methodology has commonly been applied to  
477 trace particles to abstraction wells for the purpose of wellhead protection due to  
478 uncertainties related to constraining the fracture network even in heavily fractured  
479 sandstones (e.g., Freeze and Cherry 1979). The use of the EPM is reasonable for particle  
480 tracking and contaminant transport purposes at a variety of scales where the Sherwood  
481 Sandstone Aquifer is porous and dominated by matrix flow (the case of the upper-right  
482 portion of the panel). Here, the REV is small, and values of core plugs can be used to  
483 calibrate groundwater flow models. Notably, the Sherwood Sandstone Aquifer has been  
484 modelled across the Great Britain using the EPM approach as a single hydraulic unit for  
485 contaminant transport purposes (Knipe et al. 1993; Allen et al. 1998; Seymour et al. 2006;  
486 Bottrell et al. 2006). This assumption (Figure 8, right-upper portion of the panel) is certainly  
487 reasonable in the case of the Eastern England Shelf where the sandstone is highly porous,

488 relatively homogeneous, no individual stratigraphic members are identifiable and aeolian  
489 lithofacies are absent (Ambrose et al. 2014; Wakefield et al. 2015; Medici et al. 2019a).  
490 However, where present we recommend the use of contrasting values of EPM effective  
491 porosity to characterize aeolian and fluvial units separately, with aeolian-dominated  
492 deposits such as the Helsby Sandstone and the Ormskirk Sandstone formations of the  
493 Cheshire and Eastern Irish Sea basins characterized by higher values of effective porosity.  
494 Such formations of primary aeolian origin are more porous and permeable at the core-plug  
495 scale and less heavily fractured compared to fluvial-dominated formations (Fig. 7; Allen et  
496 al. 1997; Tellam and Barker 2006; Medici et al. 2018). This difference arises because the  
497 aeolian dune sandstones are petro-physically different from fluvial channel sandstones as  
498 shown by wireline logging in the Sellafield. Here, the Triassic aeolianites are characterized  
499 by a dominant component of matrix flow (Jones and Ambrose 1994; Sutton 1996).

500 In contrast, fluvial units may be fracture-flow dominated where the Sherwood Sandstone  
501 Aquifer has relatively high mechanical resistance. The fracturing network can be spatially  
502 constrained and modelled using a DFN-M approach at scales of less than  $\sim 10 \text{ km}^2$  in  
503 systems where fracture flow is important (see right-central portion of the panel in Figure 8).  
504 This approach may provide model simulation benefits to be used in the Sherwood  
505 Sandstone in the Cheshire Basin, allowing representation of both chemical advection and  
506 diffusivity in the fractures and matrix blocks, respectively to model contaminant transport.  
507 To allow representation of this complexity, a network of discrete flowing fractures need to  
508 be inserted in an EPM in sandstone aquifers as proposed by Pierce et al. (2018) and  
509 illustrated in the right-central portion of the panel in Figure 8.

510 DFN solutions should also be considered where geomechanical effects, e.g. stress  
511 changes within the disturbed zones around tunnels and excavations could potentially  
512 influence hydraulic conductivity via increasing fracture apertures. A geomechanical  
513 approach to DFN modelling can be used in the future in the high-mechanically resistant

514 areas of the Sherwood Sandstone Aquifer. This rock-type is subject to large excavations in  
515 west Cumbria, Lancashire and Merseyside to meet the demands of the UK national market  
516 for building stones (Yates 1992).

517 A one end of the spectrum of hydraulic behaviours that the Sherwood Sandstone Aquifer  
518 shows across the Great Britain, this aquifer locally behaves as moderately (pseudo-)  
519 karstified with occurrence of conduits 0.05-0.6 m large. This sandstone is characterized by  
520 a transmissive zone in the first 100-150 m below the ground in west Cumbria (Streetly et  
521 al. 2000). Here, the transmissivity ( $1.0 \times 10^{-1} \text{ m}^2/\text{s}$ ) is much higher in valleys with axis of 2 km  
522 and at this scale conduits should be inserted in groundwater flow models (Figure 8 lower-  
523 right portion of the panel). Additionally, high ( $\sim 10^{-3} \text{ m/s}$ ) flow velocities characteristic of  
524 karstic carbonate systems were identified in the Sherwood Sandstone of the Liverpool  
525 area (Barker et al. 1998). The use of the Darcy-Weisbach equations (mathematical details  
526 in Valiantzas 2008) that describe laminar and turbulent flow in discrete pipe-conduit  
527 elements may be appropriate here. More research is needed to verify the widespread  
528 presence of karst-like conduits in the Sherwood Sandstone Aquifer in NW England. New  
529 tracer tests in the highly transmissive valleys in west Cumbria might reveal higher flow  
530 velocities than  $1.6 \times 10^{-3} \text{ m/s}$  found in Liverpool by Barker et al. (1998). More tracer testing  
531 would also determine the effective porosity which is inadequately characterised in the  
532 Sherwood Sandstone Aquifer and is necessary to run contaminant transport models (Allen  
533 et al. 1997; Tellam and Barker 2006; Medici and West 2021). Note that, values of effective  
534 porosity used to run contaminant transport models in the range 0.1 - 0.35 and are not  
535 experimentally supported (Bottrell et al. 2006; Rivett et al. 2012; Zhang et al. 2010, 2011,  
536 2016). Much lower values are expected in the Sherwood Sandstone Aquifer of north-west  
537 England. In this area, groundwater flow is largely dominated by bedding plane fractures.  
538 Fracture flow aquifers are characterized by effective porosities in the range  $\sim 10^{-3}$  -  $\sim 10^{-5}$   
539 (Ren et al. 2018; Medici and West 2021; Moore and Walsh 2021).

540 To treat fractured aquifers with occurrence of some conduits, the hydrogeologists of the  
541 USGS have applied the Darcy-Weisbach solution to MODFLOW-2005, and they found the  
542 models are highly sensitive to the diameter of conduits (Valiantzas 2008; Shoemaker et al.  
543 2008; Hill et al. 2010; Gallegos et al. 2013; Saller et al. 2013; Medici et al. 2019b).  
544 According to the methodology of the USGS, the Darcy-Weisbach equations need to be  
545 embedded and either DFN or EPM codes are used to model groundwater flow away from  
546 such conduits in sandstones (right-lower portion of the panel in Figure 8). This  
547 methodology can be used in the Sherwood Sandstone Aquifer of north-western England at  
548 the sites where conduits are identified by tracer testing, pumping tests, optical and  
549 acoustic televiewer logs or inferred from geomorphological surveys.

550

551

## 552 **Conclusions**

553 The fluvio-aeolian deposits of the Sherwood Sandstone Aquifers across Great Britain are  
554 complex from a hydrogeological point of view as demonstrated by core plug tests, field  
555 pumping tests, borehole fluid logging analysis and tracer testing. Consequently, three  
556 different approaches to groundwater flow modelling: EPM, DFN and CN modelling need to  
557 be considered for these and other sandstone aquifer-types, depending on modelling  
558 objectives, observation scale, degree of heterogeneities and nature of permeability. The  
559 findings of the review can be summarized as follows.

560

- 561 1. The Sherwood Sandstone Aquifer of Great Britain behaves as a matrix flow aquifer  
562 in the Eastern England Shelf, as well as the Wessex, Worcester, Needwood and  
563 Staffordshire basins, i.e.  $K_{\text{well-test}}/K_{\text{core-plug}} < 2$ . Here, the EPM approach can be used  
564 to model both groundwater flow and contaminant transport at a range of scales. The  
565 Sherwood Sandstone Aquifer is particularly homogeneous in the Eastern England

566 Shelf and characterized by exclusively fluvial deposits. Thus, use of a single layer  
567 with EPM properties can characterize the grid.

568 2. Multiple hydraulic-units should be modelled for contaminant transport purposes  
569 where both fluvial and aeolian deposits form part of the groundwater system.  
570 Aeolian lithofacies are more porous and less densely fractured than fluvial units,  
571 and likely are dominated by matrix flow. Hence, such deposits need to be  
572 characterized by higher effective porosities in EPM models, which implies that  
573 contaminant dispersal is likely to be slower than in deposits of fluvial origin.

574 3. Fractures represent the principal flow pathways in the Sherwood Sandstone Aquifer  
575 of the Cheshire and Eastern Irish Sea Basin. Here, either EPM or DFN models may  
576 be appropriate, depending on the modelling scale and the extent of available  
577 information on the conductive fracture network. For large scale (defined here as >  
578 10 km<sup>2</sup>) modelling areas, a EPM approach, with an appropriate number of layers  
579 to correctly represent both fracture and matrix flow units, may be the only practicable  
580 approach. For smaller scale models (plan area < 10 km<sup>2</sup>, but including much  
581 smaller domains), a DFN approach may be considered, which accounts for both  
582 chemical advection and diffusion in fractures and matrix, respectively. Similar  
583 approaches have been applied to siliciclastic rocks in California, Colorado and  
584 Wisconsin.

585 4. Tracer tests indicate karst-like velocities in the Sherwood Sandstone Aquifer in the  
586 north-west of England. Cavities with apertures 0.05 - 0.60 m have been detected,  
587 where calcite cements have been dissolved in correspondence of fractures, similar  
588 to limestone or dolostone aquifers. In such scenarios, the Sherwood Sandstone  
589 Aquifer can be modelled by embedding discrete conduits elements in a DFN-M with  
590 flowing pores and fractures, to appropriately simulate the karst-like flow velocities  
591 detected by tracer testing.



592

593 Overall, the review has shown that aquifers developed in the Triassic Sherwood  
594 Sandstone Aquifer exhibits a spectrum of hydraulic behaviours from matrix, to fracture flow  
595 with secondary intergranular porosity, up to moderately karst-like behaviour.  
596 Consequently, various flow modelling approaches may be appropriate. Further field  
597 studies to determine effective porosity and assess characteristics of fractures and scale of  
598 conduit networks are recommended to support contaminant transport models in these  
599 aquifers, and similarly for analogous sandstones worldwide.

600

### 601 **Acknowledgement**

602 The results of this study benefitted from discussions with Ferdinando Manna and Stephen  
603 Foster at the University of Guelph (Canada) and University of Leeds (UK), respectively.  
604 The manuscript finds inspiration from an industrially funded project supported by  
605 TotalEnergies. In this framework, we are particularly grateful to Phillipe Ruelland  
606 (TotalEnergies, France) and Nigel Mountney (University of Leeds) for their support and  
607 discussions. Finally, the manuscript benefitted from constructive review comments of two  
608 anonymous reviewers, Associate Editor Jonathan Smith (Shell, Netherlands), and  
609 Matthijs Bonte (VU University Amsterdam, Netherlands).

610

### 611 **Bibliography**

612 Abesser C. and Lewis M. 2015. A semi-quantitative technique for mapping potential  
613 aquifer productivity on the national scale: example of England and Wales (UK).  
614 Hydrogeology Journal, 23, 1677-1694.

- 615 Allen, D.J., Bloomfield, J.P., Gibbs, B.R. and Wagstaff, S.J. 1998. Fracturing and the  
616 hydrogeology of the Permo-Triassic sandstones in England and Wales. Technical Report  
617 WD/98/1, Nottingham, British Geological Survey.
- 618 Allen, D.J., Brewerton, L.M., Coleby, B.R., Gibbs, M.A., Lewis, A.M., MacDonald S.J.,  
619 Wagstaff A.T. and Williams L.J. 1997. The Physical Properties of Major Aquifers in  
620 England and Wales. Technical Report WD/97/34, Nottingham, British Geological Survey.
- 621 Ambrose, K., Hough, E., Smith, N.J.P. and Warrington, G. 2014. Lithostratigraphy of the  
622 Sherwood Sandstone Group of England, Wales and south-west Scotland. Technical  
623 Report RR/14/001, British Geological Survey, Nottingham (UK).
- 624 Aydin, A. 2000. Fractures, faults, and hydrocarbon entrapment, migration and flow. *Marine*  
625 *and Petroleum Geology*, 17, 797-814.
- 626 Balin, D.F. 2000. Calcrete morphology and karst development in the upper Old Red  
627 Sandstone at Milton Ness, Scotland. Geological Society, London, Special  
628 Publications, 180, 485-501.
- 629 Banks, D., Withers, J. G., Cashmore, G. and Dimelow, C. 2013. An overview of the results  
630 of 61 in situ thermal response tests in the UK. *Quarterly Journal of Engineering Geology*  
631 *and Hydrogeology*, 46, 281-291.
- 632 Barker, A.P., Newton, R.J., Bottrell, S.H. and Tellam, J.H. 1998. Processes affecting  
633 groundwater chemistry in a zone of saline intrusion into an urban sandstone aquifer.  
634 *Applied Geochemistry*, 13, 735-749.
- 635 Bashar, K. and Tellam, J.H. 2011. Sandstones of unexpectedly high diffusibility. *Journal of*  
636 *Contaminant Hydrology*, 122, 40-52.

- 637 Bense, V.F., Gleeson, T., Loveless, S.E., Bour, O. and Scibek, J. 2013. Fault zone  
638 hydrogeology. *Earth-Science Reviews*, 127, 171-192.
- 639 Bishop K.R. and K.R. Rushton, 1993. Summary of the Final Report for the  
640 Nottinghamshire Sherwood Sandstone Aquifer Mathematical Modelling Investigation.  
641 University of Birmingham, Birmingham (UK).
- 642 Black, J.H. and Brightman, M.A. 1996. Conceptual model of the hydrogeology of  
643 Sellafeld. *Quarterly Journal of Engineering Geology and Hydrogeology*, 29, 83-93.
- 644 Bloomfield, J. P. and Williams, A.T. 1995. An empirical liquid permeability—gas  
645 permeability correlation for use in aquifer properties studies. *Quarterly Journal of*  
646 *Engineering Geology and Hydrogeology*, 28, 143-150.
- 647 Bloomfield, J.P., Moreau, M.F. and Newell, J. 2006. Characterization of permeability  
648 distributions in six lithofacies from the Helsby and Wilmslow sandstone formations.  
649 Geological Society, London, Special Publications, 263, 83-101.
- 650 Bottrell, S.H., West, L.J. and Yoshida, K. 2006. Combined isotopic and modelling  
651 approach to determining the source of saline groundwaters in the Selby Triassic sandstone  
652 aquifer, UK. Geological Society, London, Special Publications, 263, 325-338.
- 653 Bottrell, S., Tellam, J., Bartlett, R. and Hughes, A. 2008 Isotopic composition of sulfate as  
654 a tracer of natural and anthropogenic influences on groundwater geochemistry in an urban  
655 sandstone aquifer, Birmingham, UK. *Applied Geochemistry*, 23, 2382-2394.
- 656 Bouch, J.E., Hough, E., Kemp, S.J., McKervey, J.A., Williams, G.M. and Greswell, R.B.  
657 2006. Sedimentary and diagenetic environments of the Wildmoor Sandstone Formation  
658 (UK): implications for groundwater and contaminant transport, and sand  
659 production. Geological Society, London, Special Publications, 263, 129-153.

- 660 Brassington, F.C. and Walthall, S. 1985. Field techniques using borehole packers in  
661 hydrogeological investigations. Quarterly Journal of Engineering Geology and  
662 Hydrogeology, 18, 181-193.
- 663 Brookfield, M.E. 2008. Palaeoenvironments and palaeotectonics of the arid to hyperarid  
664 intracontinental latest Permian-late Triassic Solway basin (UK). Sedimentary Geology,  
665 210, 27-47.
- 666 Burley, S.D. 1984. Patterns of diagenesis in the Sherwood Sandstone Group (Triassic),  
667 United Kingdom. Clay Minerals, 19, 403-440.
- 668 Carminati, E., Cuffaro, M. and Doglioni, C. 2009. Cenozoic uplift of Europe. Tectonics,  
669 28(4).
- 670 Chadwick, R.A. and Evans, D.J. 1995. The timing and direction of Permo-Triassic  
671 extension in southern Britain. Geological Society, London, Special Publications, 91, 161-  
672 192.
- 673 Colyer, A., Butler, A., Peach, D. and Hughes, A. 2021. How groundwater time series and  
674 aquifer property data explain heterogeneity in the Permo-Triassic sandstone aquifers of  
675 the Eden Valley, Cumbria, UK. Hydrogeology Journal, [https://doi.org/10.1007/s10040-021-](https://doi.org/10.1007/s10040-021-02437-6)  
676 02437-6.
- 677 Cook, P.G. 2003. A guide to regional groundwater flow in fractured rock aquifers. Seaview  
678 Press, West Lakes, Australia.
- 679 Davison, R.M. and Lerner, D.N. 2000. Evaluating natural attenuation of groundwater  
680 pollution from a coal-carbonisation plant: developing a local-scale model using  
681 MODFLOW, MODTMR and MT3D. Water and Environment Journal, 14, 419-426.

- 682 Daw G.P., Howell F.T. and Woodhead G.A. 1974. The effect of applied stress upon the  
683 permeability of some Permian and Triassic sandstones of northern England. *International*  
684 *Journal of Rock Mechanics and Mining Science Abstracts*, 13, 537–542.
- 685 Day-Lewis, F.D., Johnson, C.D., Paillet, F.L. and Halford, K.J. 2011. A computer program  
686 for flow-log analysis of single holes (FLASH). *Groundwater*, 49, 926-931.
- 687 Ford, M. and Tellam, J.H. 1994. Source, type and extent of inorganic contamination within  
688 the Birmingham urban aquifer system, UK. *Journal of Hydrology*, 156, 101-135.
- 689 Foster, S., West, L., Bottrell, S. and Hildyard, M.W. 2018. A DFN Approach to Evaluating  
690 the Hydrogeological Significance of Lithostatic Unloading in Fractured Strata Around  
691 Open-Pit Workings. In: 2nd International Discrete Fracture Network Engineering  
692 Conference Extended Abstracts. OnePetro, Texas (USA).
- 693 Freeze, R.A. and Cherry J.A. 1979. *Groundwater*. Prentice-Hall, Hoboken, New Jersey,  
694 USA.
- 695 Gallegos, J.J., Hu, B.X., and Davis H. 2013. Simulating flow in karst aquifers at laboratory  
696 and sub-regional scales using MODFLOW-CFP. *Hydrogeology Journal*, 21, 1749-1760.
- 697 GeoMappApp 2021. Version 3.6.14. Earth Observatory of the Columbia University, New  
698 York State, New York, USA.
- 699 Gooddy, D. C., Stuart, M. E., Lapworth, D. J., Chilton, P. J., Bishop, S., Cachandt, G.,  
700 Knapp M. and Pearson, T. 2005. Pesticide pollution of the Triassic Sandstone aquifer of  
701 South Yorkshire. *Quarterly Journal of Engineering Geology and Hydrogeology*, 38, 53-63.
- 702 Gogu, R.C., Hallet, V. and Dassargues, A. 2003. Comparison of aquifer vulnerability  
703 assessment techniques. Application to the Néblon river basin (Belgium). *Environmental*  
704 *Geology*, 44, 881-892.

- 705 Gutmanis, J.C., Lanyon, G.W., Wynn, T.J. and Watson, C.R. 1998. Fluid flow in faults: a  
706 study of fault hydrogeology in Triassic sandstone and Ordovician volcanoclastic rocks at  
707 Sellafeld, north-west England. *Proceeding of the Yorkshire Geological Society*, 52,159-  
708 175.
- 709 Harris, R. C. and Lowe, D.R. 1984. Changes in the organic fraction of leachate from two  
710 domestic refuse sites on the Sherwood Sandstone, Nottinghamshire. *Quarterly Journal of*  
711 *Engineering Geology and Hydrogeology*, 17, 57-69.
- 712 Hartmann, A., Goldscheider, N., Wagener, T., Lange, J. and Weiler, M. 2014. Karst water  
713 resources in a changing world: Review of hydrological modeling approaches. *Reviews of*  
714 *Geophysics*, 52, 218-242.
- 715 Hill, M.C. and Tiedeman C.R. 2006. *Effective groundwater model calibration: with analysis*  
716 *of data, sensitivities, predictions, and uncertainty*. John Wiley & Sons, Hoboken, USA.
- 717 Hill, M.E., Stewart, M.T. and Martin A. 2010. Evaluation of the MODFLOW-2005 conduit  
718 flow process. *Groundwater*, 48, 549-559.
- 719 Hitchmough, A.M., Riley, M.S., Herbert, A.W. and Tellam J.H. 2007. Estimating the  
720 hydraulic properties of the fracture network in a sandstone aquifer. *Journal of Contaminant*  
721 *Hydrology*, 93, 38-57.
- 722 Hudson M. 2008. *Groundwater Asset Maintenance*. Geological Society, Hydro-group  
723 online presentations. South Staff Water, Walsall, UK.
- 724 Jaber, F.H. and Shukla, S. 2012. MIKE SHE: Model use, calibration, and  
725 validation. *Transactions of the ASABE*, 55, 1479-1489.

- 726 Jones, N.S. and Ambrose, K. 1994. Triassic sandy braidplain and aeolian sedimentation in  
727 the Sherwood Sandstone Group of the Sellafield area, west Cumbria. Proceedings of the  
728 Yorkshire Geological Society, 50, 61-76.
- 729 Knipe, C.V., Lloyd, J.W., Lerner, D.N. and Greswell, R. 1993. Rising Groundwater in  
730 Birmingham and the Engineering Implications. Construction Industry Research and  
731 Information Association (CIRIA) Spec. Pub. 92. London, UK.
- 732 Kortas, L. and Younger P.L. 2013. Fracture patterns in the Permian Magnesian limestone  
733 aquifer, Co. Durham, UK. Proceedings of the Yorkshire Geological Society, 59, 161-171.
- 734 Kůrková, I., Bruthans, J., Balák, F., Slavík, M., Schweigstilllová, J., Bruthansová, J., Mikuš,  
735 P., Vojtíšek, J. and Grundloch, J. 2019. Factors controlling evolution of karst conduits in  
736 sandy limestone and calcareous sandstone (Turnov area, Czech Republic). Journal of  
737 Hydrology, 574, 1062-1073.
- 738 Manna, F., Murray, S., Abbey, D., Martin, P., Cherry, J. and Parker, B. 2019. Spatial and  
739 temporal variability of groundwater recharge in a sandstone aquifer in a semiarid  
740 region. Hydrology and Earth System Sciences, 23, 2187-2205.
- 741 McKie, T. and Williams, B. 2009. Triassic palaeogeography and fluvial dispersal across the  
742 northwest European Basins. Geological Journal, 44, 711-741.
- 743 McKoy, M.L. and Sams N.W. 1997. Tight gas reservoir simulation: Modeling discrete  
744 irregular strata-bound fracture networks and network flow, including dynamic recharge  
745 from the matrix. In: Proceedings of the Natural Gas Conference Emerging Technologies  
746 for the Natural Gas Industry. US Department of Energy's Federal Energy Technology  
747 Center Publication. Washington DC, USA.

- 748 Medici, G., Boulesteix, K., Mountney, N.P., West, L.J. and Odling, N.E. 2015.  
749 Palaeoenvironment of braided fluvial systems in different tectonic realms of the Triassic  
750 Sherwood Sandstone Group, UK. *Sedimentary Geology*, 329, 188-210.
- 751 Medici, G., L.J. West, and Mountney N.P. 2016. Characterizing flow pathways in a  
752 sandstone aquifer: Tectonic vs sedimentary heterogeneities. *Journal of Contaminant*  
753 *Hydrology*, 194, 36-58.
- 754 Medici, G., West, L.J. and Mountney N.P. 2018. Characterization of a fluvial aquifer at a  
755 range of depths and scales: the Triassic St Bees Sandstone Formation, Cumbria, UK.  
756 *Hydrogeology Journal*, 26, 565-591.
- 757 Medici, G., West, L.J. and Mountney, N.P. 2019a. Sedimentary flow heterogeneities in the  
758 Triassic UK Sherwood Sandstone Group: Insights for hydrocarbon exploration. *Geological*  
759 *Journal*, 54, 1361-1378.
- 760 Medici, G., West, L.J., Mountney, N.P. and Welch, M. 2019b. Permeability of rock  
761 discontinuities and faults in the Triassic Sherwood Sandstone Group (UK): insights for  
762 management of fluvio-aeolian aquifers worldwide. *Hydrogeology Journal*, 27(8), 2835-  
763 2855.
- 764 Medici, G., Smeraglia, L., Torabi, A. and Botter, C. 2021. Review of Modeling Approaches  
765 to Groundwater Flow in Deformed Carbonate Aquifers. *Groundwater*, 59, 334-351.
- 766 Medici, G. and West, L. J. 2021. Groundwater flow velocities in karst aquifers; importance  
767 of spatial observation scale and hydraulic testing for contaminant transport prediction.  
768 *Environmental Science and Pollution Research*, 28, 43050-43063.



- 769 Meus, P. and Willems, L. 2021. Tracer tests to infer the drainage of the multiple porosity  
770 aquifer of Luxembourg Sandstone (Grand-Duchy of Luxembourg): implications for drinking  
771 water protection. *Hydrogeology Journal*, 29, 461-480.
- 772 Miller, I., Lee, G., Dershowitz, W. and Sharp G. 1994. MAFIC - Matrix/Fracture Interaction  
773 Code with Solute Transport. User Documentation, Version 1.5. Golder Associates, Inc.  
774 Report 923-1089, Seattle (USA).
- 775 Moore, J.P. and Walsh, J.J. 2021. Quantitative analysis of Cenozoic faults and fractures  
776 and their impact on groundwater flow in the bedrock aquifers of Ireland. *Hydrogeology*  
777 *Journal*, 29, 2613-2632.
- 778 Morgan C. 2019. Fracture Network Characterization of an Aquitard Surface within the  
779 Wonewoc Sandstone using Digital Outcrop Photogrammetry and Discrete Fracture  
780 Network (DFN) Modelling. PhD Thesis, University of Guelph (Canada).
- 781 Mountney, N.P. and Thompson, D.B. 2002. Stratigraphic evolution and preservation of  
782 aeolian dune and damp/wet interdune strata: an example from the Triassic Helsby  
783 Sandstone Formation, Cheshire Basin, UK. *Sedimentology*, 49, 805-833.
- 784 Neumann, I. and Hughes A. 2003. Translation of the Doncaster Groundwater Model into  
785 the MODFLOW code. Report CR/03/258N, British Geological Survey, Nottingham (UK).
- 786 Newell, A.J. 2018. Rifts, rivers and climate recovery: A new model for the Triassic of  
787 England. *Proceedings of the Geologists' Association*, 129, 352-371.
- 788 Odling, N.E., Gillespie, P., Bourgine, B., Castaing, C., Chiles, J. P., Christensen, N. P. and  
789 Watterson, J. 1999. Variations in fracture system geometry and their implications for fluid  
790 flow in fractures hydrocarbon reservoirs. *Petroleum Geoscience*, 5, 373-384.

- 791 Offerdinger, U., MacDonald, A.M., Comte, J.C. and Young, M.E. 2019. Groundwater in  
792 fractured bedrock environments: managing catchment and subsurface resources—an  
793 introduction. Geological Society, London, Special Publications, 479, 1-9.
- 794 Parker B.L., K. Bairos, C.H. Maldaner, S.W. Chapman, C.M. Turner, L.S. Burns, J. Plett,  
795 R. Carter, and Cherry J.A. 2019. Metolachlor dense non-aqueous phase liquid source  
796 conditions and plume attenuation in a dolostone water supply aquifer. Geological Society,  
797 London, Special Publications, 479, 207-236.
- 798 Pierce, A.A., Chapman, S.W., Zimmerman, L.K., Hurley, J.C., Aravena, R., Cherry, J.A.  
799 and Parker, B.L. 2018. DFN-M field characterization of sandstone for a process-based site  
800 conceptual model and numerical simulations of TCE transport with degradation. Journal of  
801 Contaminant Hydrology, 212, 96-114.
- 802 Pilato, T. 2021. Exploring the Statistical Method of Moments for Solute Transport in  
803 Fractured Porous Rock Aquifers: Bridging the Gap between Local and Regional Scales.  
804 MSc Thesis, University of Guelph (Canada).
- 805 Pokar, M., West, L.J. and Odling, N.E. 2006. Petrophysical characterization of the  
806 Sherwood sandstone from East Yorkshire, UK. Geological Society, London, Special  
807 Publications, 263, 103-118.
- 808 Powell, K.L., Taylor, R.G., Cronin, A.A., Barrett, M.H., Pedley, S., Sellwood, J., Trowsdale,  
809 S.A. and Lerner, D.N. 2003. Microbial contamination of two urban sandstone aquifers in  
810 the UK. Water Research, 37, 339-352.
- 811 Ramingwong, T. 1974. Hydrogeology of the Keuper sandstone in the Droitwich syncline  
812 area-Worcestershire. PhD thesis, University of Birmingham (UK).

- 813 Ren, S., Gragg, S., Zhang, Y., Carr, B.J. and Yao, G. 2018. Borehole characterization of  
814 hydraulic properties and groundwater flow in a crystalline fractured aquifer of a headwater  
815 mountain watershed, Laramie Range, Wyoming. *Journal of Hydrology*, 561, 780-795.
- 816 Riley, M., Tellam, J., Greswell, R., Durand, V. and Aller, M.F. 2011. Convergent tracer  
817 tests in multilayered aquifers: The importance of vertical flow in the injection borehole,  
818 *Water Resources Research*, <https://doi.org/10.1029/2010WR009838>.
- 819 Rivers, C.N., Barrett, M.H., Hiscock, K.M., Dennis, P.F, Feast, N.A. and Lerner, D.N. 1996.  
820 Use of nitrogen isotopes to identify nitrogen contamination of the Sherwood Sandstone  
821 aquifer beneath the city of Nottingham, United Kingdom. *Hydrogeology Journal*, 4, 90-102.
- 822 Rivett, M. O., Smith, J. W. N., Buss, S. R. and Morgan, P. 2007. Nitrate occurrence and  
823 attenuation in the major aquifers of England and Wales. *Quarterly Journal of Engineering  
824 Geology and Hydrogeology*, 40, 335-352.
- 825 Rivett, M.O., Turner, R.J., Glibbery, P. and Cuthbert, M.O. 2012. The legacy of chlorinated  
826 solvents in the Birmingham aquifer, UK: Observations spanning three decades and the  
827 challenge of future urban groundwater development. *Journal of Contaminant Hydrology*,  
828 140, 107-123.
- 829 Rockfield 2001. *ELFEN 2D/3D numerical modelling package, version 3.0*. Rockfield  
830 Software Ltd, Swansea (UK).
- 831 Saller, S.P., Ronayne, M.J. and Long, A.J. 2013. Comparison of a karst groundwater  
832 model with and without discrete conduit flow. *Hydrogeology Journal*, 21, 1555-1566.
- 833 Schmid, S., Worden, R. H. and Fisher, Q.J. 2006. Sedimentary facies and the context of  
834 dolomite in the Lower Triassic Sherwood Sandstone group: Corrib Field west of  
835 Ireland. *Sedimentary Geology*, 187, 205-227.

- 836 Schulze-Makuch, D., Carlson, D.A., Cherkauer, D.S. and Malik, P. 1999. Scale  
837 dependency of hydraulic conductivity in heterogeneous media. *Groundwater*, 37, 904-919.
- 838 Schulze-Makuch, D. 2005. Longitudinal dispersivity data and implications for scaling  
839 behavior. *Groundwater*, 43, 443-456.
- 840 Selroos, J.O., D.D. Walker, Ström, A., Gylling, B. and Follin S. 2002. Comparison of  
841 alternative modelling approaches for groundwater flow in fractured rock. *Journal of*  
842 *Hydrology*, 257, 174-188.
- 843 Seymour, K.J., Ingram, J.A. and Gebbett, S.J. 2006. Structural controls on groundwater  
844 flow in the Permo-Triassic sandstones of NW England. Geological Society, London,  
845 Special Publication, 263, 169-185.
- 846 Shoemaker, B.W., Kuniatsky, E.L., Birk, S., Bauer, S. and Swain, E.D. 2008.  
847 Documentation of a conduit flow process (CFP) for MODFLOW-2005. Techniques and  
848 Methods. United States Geological Survey, Techniques and Methods Report, Book 6,  
849 Chapter 6 A-24.
- 850 Smedley, P.L. and Edmunds, W.B. 2002. Redox Patterns and Trace-Element Behavior in  
851 the East Midlands Triassic Sandstone Aquifer, UK. *Groundwater*, 40, 44-58.
- 852 Smith, S.A. 1990. The sedimentology and accretionary styles of an ancient gravel-bed  
853 stream: the Budleigh Salterton Pebble Beds (Lower Triassic), southwest  
854 England. *Sedimentary Geology*, 67, 199-219.
- 855 Streetly, M., Chakrabarty, C. and McLeod, R. 2000. Interpretation of pumping tests in the  
856 Sherwood Sandstone Group, Sellafield, Cumbria, UK. *Quarterly Journal of Engineering*  
857 *Geology and Hydrogeology*, 33, 281-299.

- 858 Streetly, H.R., Hamilton, A.C.L., Betts, C., Tellam, J.H. and Herbert, A.W. 2002.  
859 Reconnaissance tracer tests in the Triassic sandstone aquifer north of Liverpool,  
860 UK. *Quarterly Journal of Engineering Geology and Hydrogeology*, 35, 167-178.
- 861 Streetly, M.J., Heathcote, J.A. and Degnan, P.J. 2006. Estimation of vertical diffusivity  
862 from seasonal fluctuations in groundwater pressures in deep boreholes near Sellafield,  
863 NW England. *Geological Society, London, Special Publications*, 263, 155-167.
- 864 Strong, G.E., Milodowski, A.E., Pearce, J.M., Kemp, S.J., Prior, S.V. and Morton, A.C.  
865 1994. The petrology and diagenesis of Permo-Triassic rocks of the Sellafield area,  
866 Cumbria. *Proceedings of the Yorkshire Geological and Polytechnic Society*, 50, 77-89.
- 867 Sutton, J.S. 1996. Hydrogeological testing in the Sellafield area. *Quarterly Journal of*  
868 *Engineering Geology and Hydrogeology*, 29, 29-38.
- 869 Tellam, J.H. 1995. Hydrochemistry of the saline groundwaters of the lower Mersey Basin  
870 Permo-Triassic sandstone aquifer, UK. *Journal of Hydrology*, 165, 45-84.
- 871 Tellam, J.H. and Barker, R.D. 2006. Towards prediction of saturated-zone pollutant  
872 movement in groundwaters in fractured permeable-matrix aquifers: the case of the UK  
873 Permo-Triassic sandstones. *Geological Society Special, London, Publications*, 263, 1-48.
- 874 Thompson, D.B. 1970. Sedimentation of the Triassic (Scythian) red pebbly sandstones in  
875 the Cheshire Basin and its margins. *Geological Journal*, 7, 183-216.
- 876 Troeger, U. and Chambel, A. 2021. Topical Collection: Progress in fractured-rock  
877 hydrogeology. *Hydrogeology Journal*, 29, 2557-2560.

- 878 Valiantzas, J.D. 2008. Explicit power formula for the Darcy–Weisbach pipe flow equation:  
879 application in optimal pipeline design. *Journal of Irrigation and Drainage Engineering*, 134,  
880 454-461.
- 881 Wakefield, O.J.W., Hough, E. and Peatfield, A.W. 2015. Architectural analysis of a Triassic  
882 fluvial system; the Sherwood Sandstone of the East Midlands Shelf, UK. *Sedimentary  
883 Geology*, 327, 1-13.
- 884 Waltham, A.C. 1993. Crown hole development in the sandstone caves of  
885 Nottingham. *Quarterly Journal of Engineering Geology and Hydrogeology*, 26, 243-251.
- 886 Wealthall, G.P., Steele, A., Bloomfield, J.P., Moss, R.H. and Lerner, D.N. 2001. Sediment  
887 filled fractures in the Permo-Triassic sandstones of the Cheshire Basin: observations and  
888 implications for pollutant transport. *Journal of Contaminant Hydrology*, 50, 41-51.
- 889 Whitworth, L.G. and Turner, A.J. 1989. Rock socket piles in the Sherwood Sandstone of  
890 Central Birmingham. *Proceedings of the Conference on Piling and Deep Foundations*.  
891 Institution of Civil Engineers, London, 327-334.
- 892 Wilcock, P. 1996. The NAPSAC fracture network code. *Developments in geotechnical  
893 engineering*. 79, 529-538).
- 894 Worthington, P.F. 1977. Influence of matrix conduction upon hydrogeophysical  
895 relationships in arenaceous aquifers. *Water Resources Research*, 13, 87-92.
- 896 Worthington, S.R.H. and Ford, D.C. 2009. Self-organized permeability in carbonate  
897 aquifers. *Groundwater*, 47, 326-336.

- 898 Worthington, S.R., Smart, C.C. and Ruland, W. 2012. Effective porosity of a carbonate  
899 aquifer with bacterial contamination: Walkerton, Ontario, Canada. *Journal of*  
900 *Hydrology*, 464, 517-527.
- 901 Worthington, S.R. 2015. Diagnostic tests for conceptualizing transport in bedrock aquifers.  
902 *Journal of Hydrology*, 529, 365-372.
- 903 Worthington, S.R., Davies, G.J. and Alexander Jr., E.C. 2016. Enhancement of bedrock  
904 permeability by weathering. *Earth-Science Reviews*, 160, 188-202.
- 905 Worthington, S.R., Foley, A.E. and Soley, R.W. 2019. Transient characteristics of effective  
906 porosity and specific yield in bedrock aquifers. *Journal of Hydrology*, 578, 124129.
- 907 Wray, R.A. 1997. A global review of solutional weathering forms on quartz  
908 sandstones. *Earth-Science Reviews*, 42, 137-160.
- 909 Yang, G., Yang, Z., Zhang, X., Tian, M., Chen, A., Ge, Z., Ping Y. and Ni, Z. 2011. RS-  
910 based geomorphic analysis of Zhangjiajie Sandstone Peak Forest Geopark,  
911 China. *Journal of Cultural Heritage*, 12, 88-97.
- 912 Yates, P.G.J. 1992. The material strength of sandstones of the Sherwood Sandstone  
913 Group of north Staffordshire with reference to microfabric. *Quarterly Journal of*  
914 *Engineering Geology and Hydrogeology*, 25, 107-113.
- 915 Young, R.W. 1986. Tower karst in sandstone: Bungle Bungle massif, northwestern  
916 Australia. *Zeitschrift für Geomorphologie*, 30, 189-202.
- 917 Young, R.W. 1988. Quartz etching and sandstone karst: examples from the East  
918 Kimberleys, northwestern Australia. *Zeitschrift für Geomorphologie*, 32, 409-423.

919 Zhang, H. and Hiscock, K.M. 2010. Modelling the impact of forest cover on groundwater  
 920 resources: A case study of the Sherwood Sandstone aquifer in the East Midlands, UK.  
 921 Journal of Hydrology, 392, 136-149.

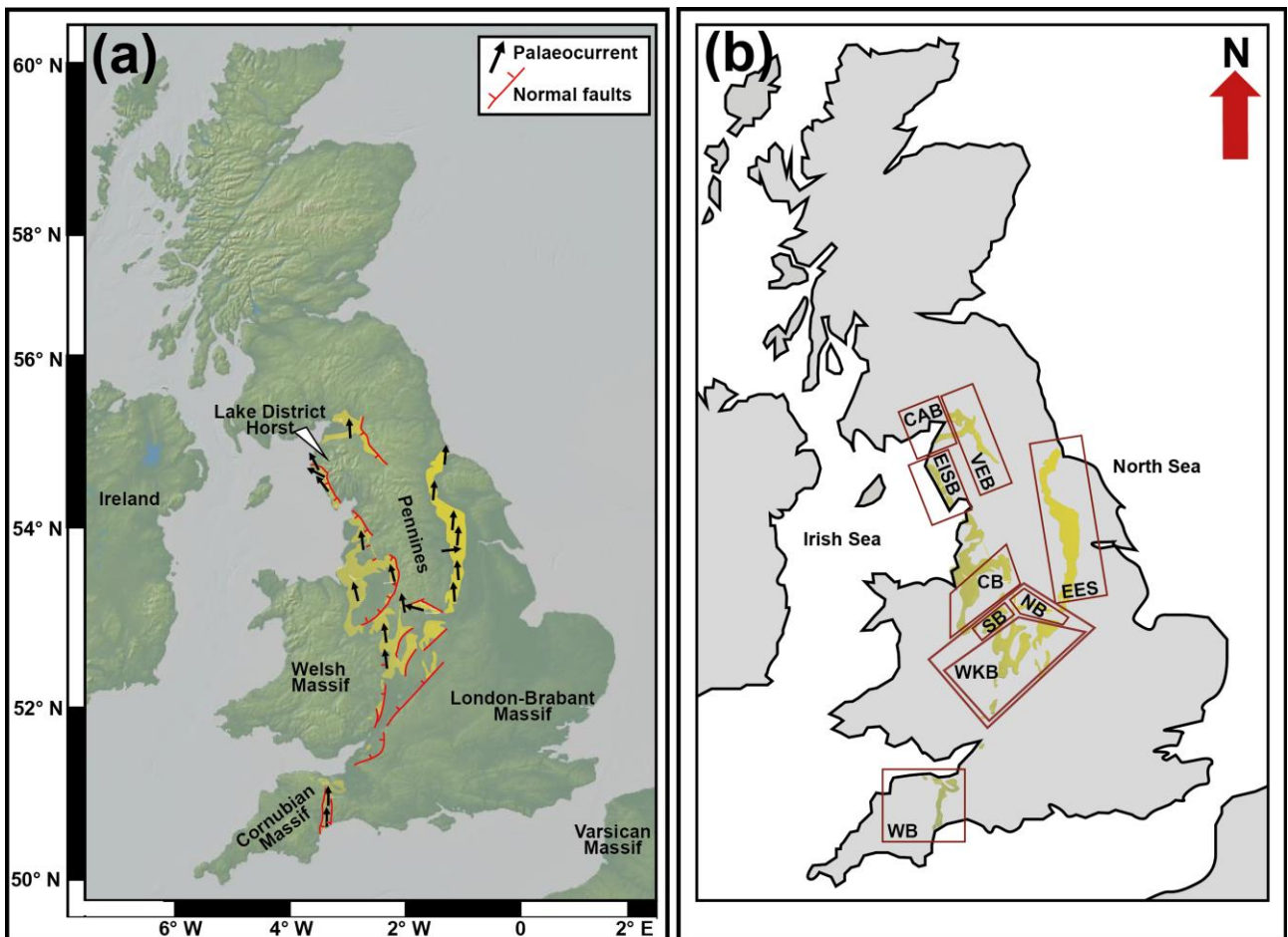
922 Zhang, H. and Hiscock, K.M. 2011. Modelling the effect of forest cover in mitigating nitrate  
 923 contamination of groundwater: A case study of the Sherwood Sandstone aquifer in the  
 924 East Midlands, UK. Journal of Hydrology, 399, 212-225.

925 Zhang, H. and Hiscock, K.M. 2016. Modelling response of groundwater nitrate  
 926 concentration in public supply wells to land-use change. Quarterly Journal of Engineering  
 927 Geology and Hydrogeology, 49, 170-182.

928

## 929 Figures

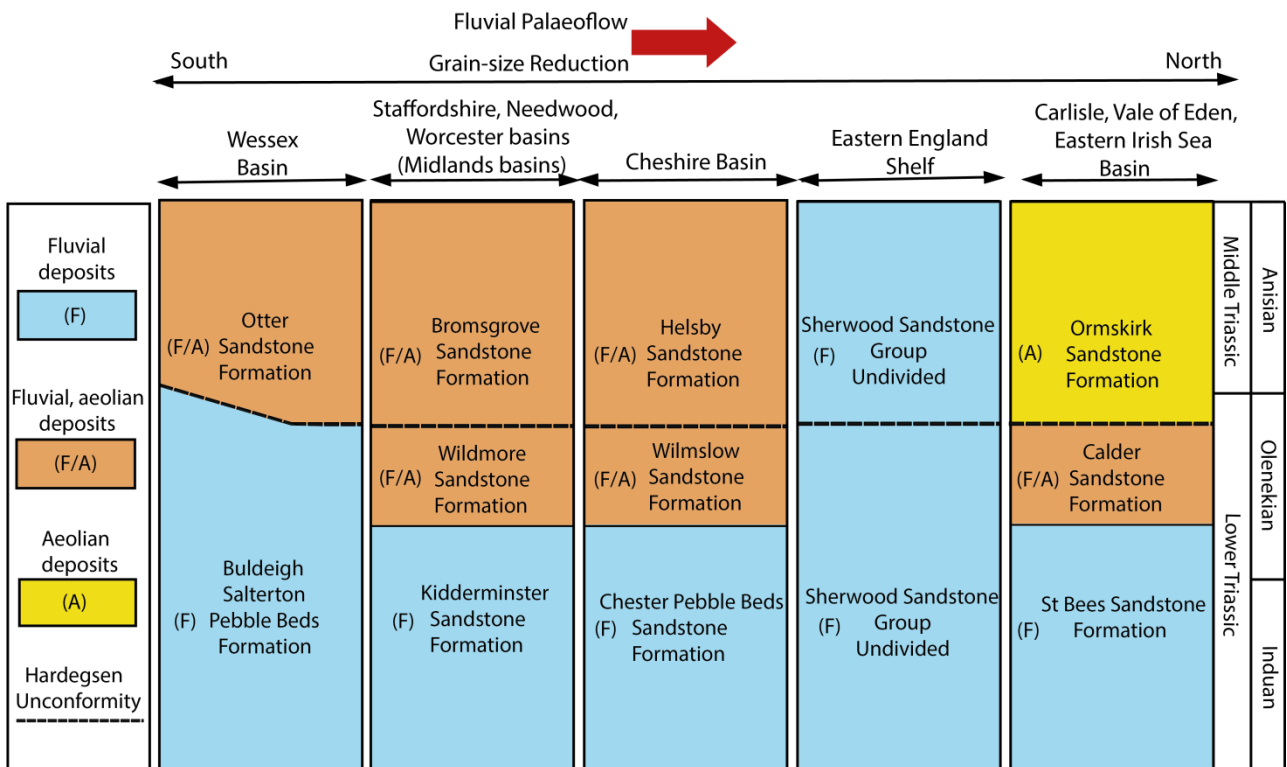
930



931

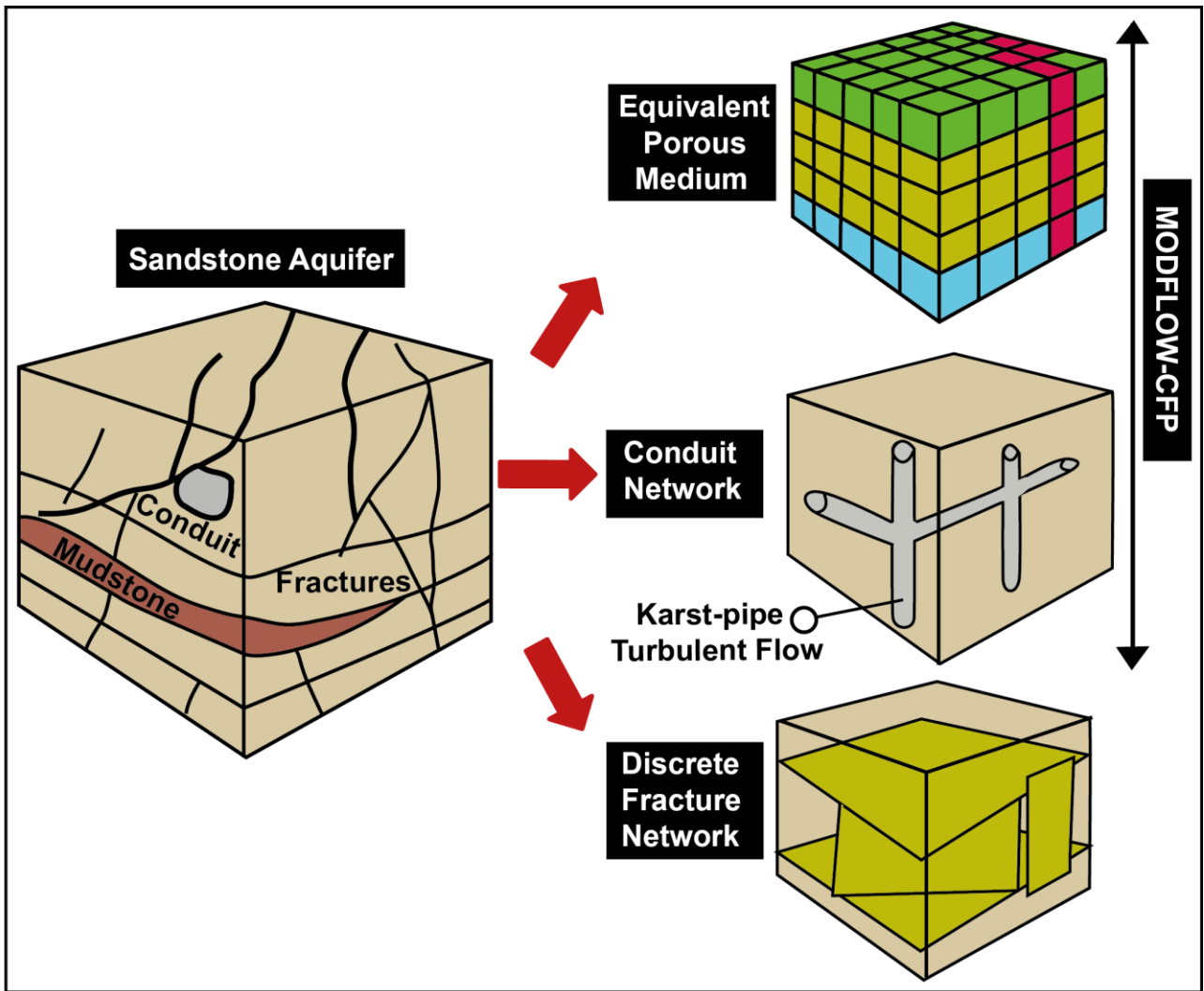


932 **Fig. 1** Siliciclastic deposits of the Sherwood Sandstone Group in England and Wales. (a)  
 933 Triassic fluvio-aeolian deposits, direction of palaeocurrents shown by arrows (basemap  
 934 from GeoMappApp 2021), (b) Triassic basins in the Great Britain: Worcester (WKB),  
 935 Staffordshire (SB), Needwood (NB), Eastern England Shelf (EES), Cheshire (CB), Eastern  
 936 Irish Sea (EISB), Vale of Eden (VEB), Wessex (WB) and Carlisle (CAB) basins (adapted  
 937 from Wakefield 2015)  
 938



939  
 940 **Fig. 2** Litho-stratigraphic scheme and nomenclature of the Triassic Sherwood Sandstone  
 941 Group in the Triassic Basins of Great Britain (adapted from Ambrose et al. 2014 and  
 942 Medici et al. 2019b).

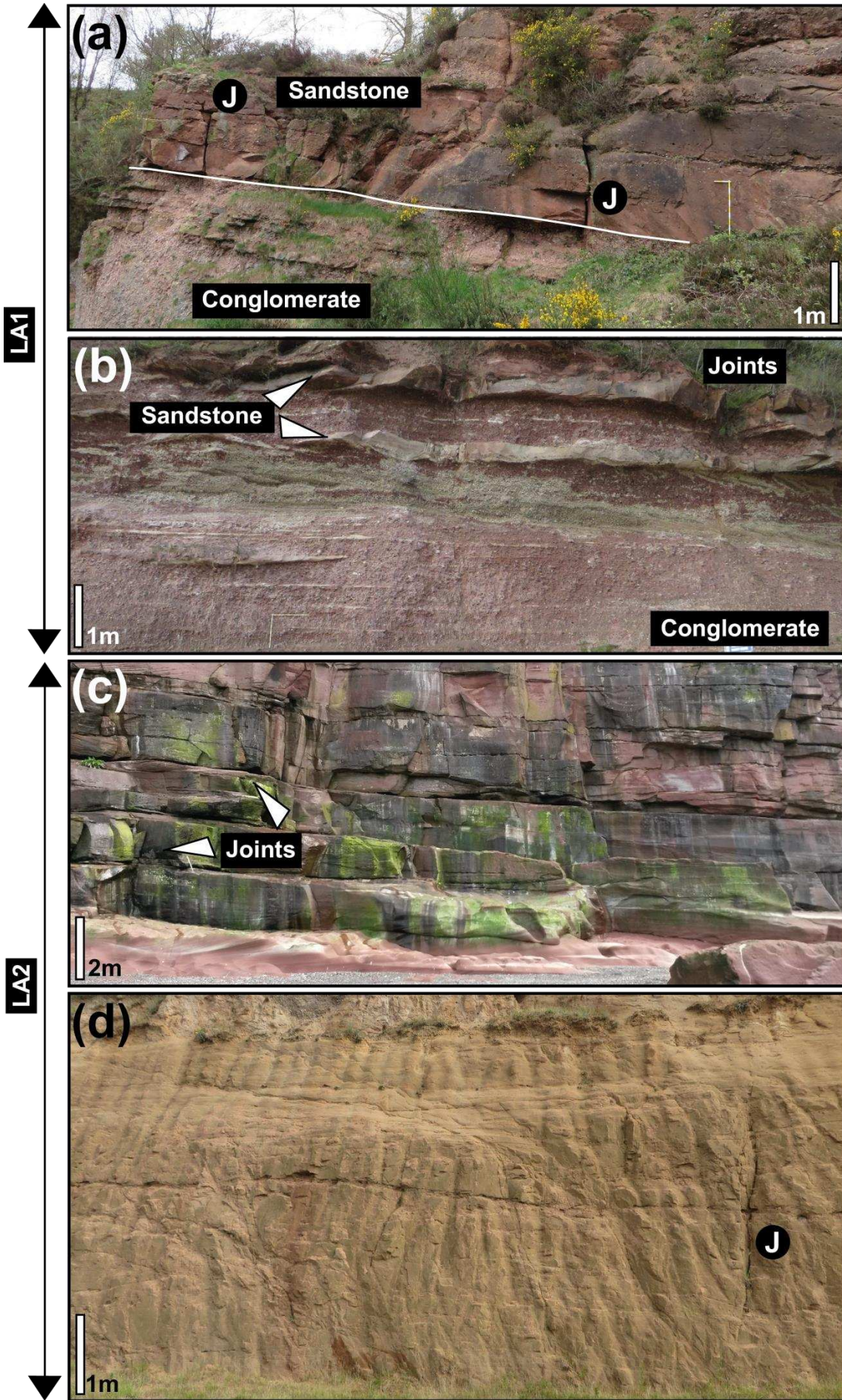
943  
 944  
 945  
 946  
 947



948

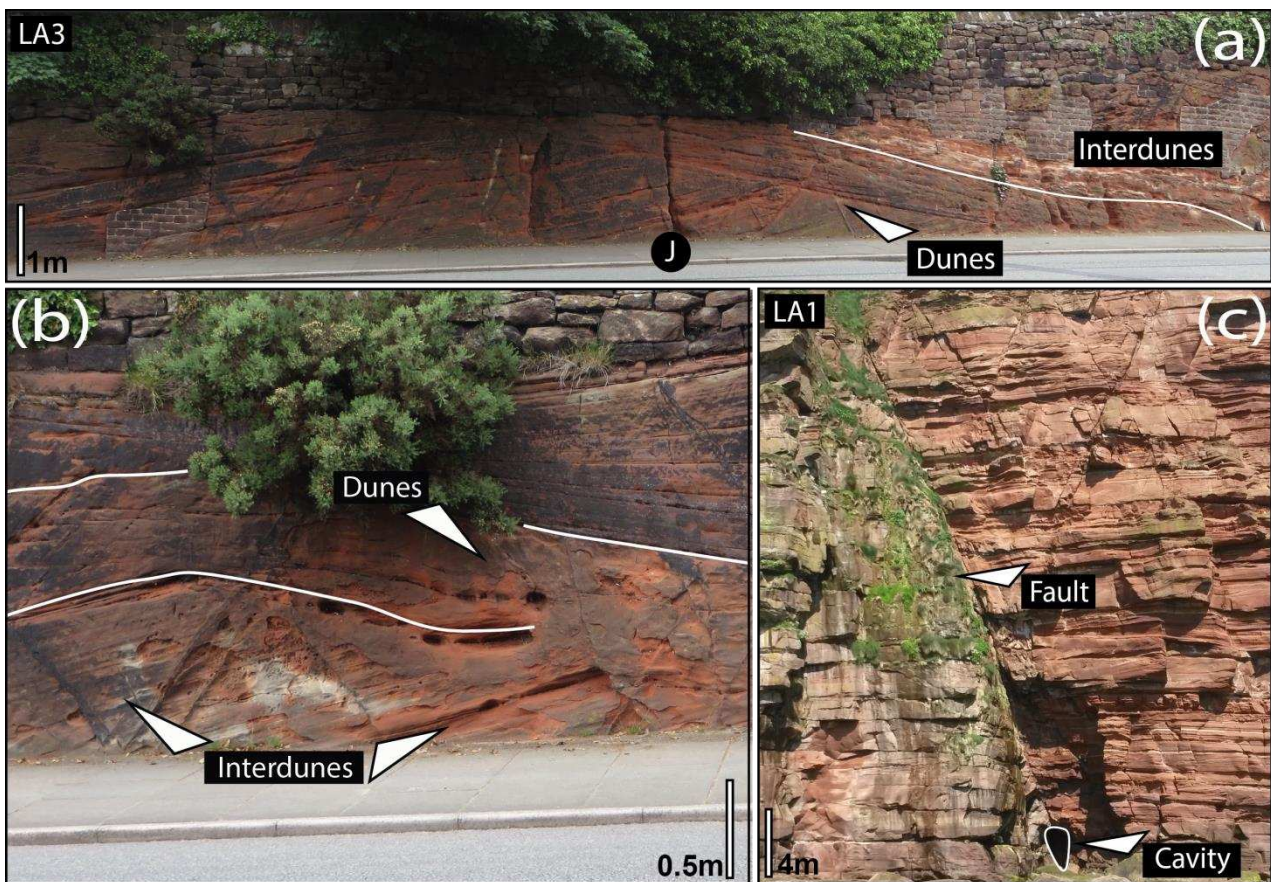
949 **Fig. 3** Conceptual model of a sandstone aquifer and the EPM, CN and DFN approaches to  
 950 numerical flow modelling (adapted from Selroos et al. 2002 and Medici et al. 2021).

951



953 **Fig. 4** Outcropping lithofacies associations (LA1, 2) in the fluvial deposits of the Sherwood  
 954 Sandstone aquifer in England. (a) Kidderminster Sandstone Formation in the Needwood  
 955 Basin, Hulme Quarry, Stoke on Trent, (b) Kidderminster Sandstone Formation in the  
 956 Staffordshire Basin, Croxden Quarry, Staffordshire, (c) St Bees Sandstone Formation,  
 957 Fleswick Bay, west Cumbria, (d) Undivided Sherwood Sandstone Group, Dunsville Quarry,  
 958 Doncaster, South Yorkshire.

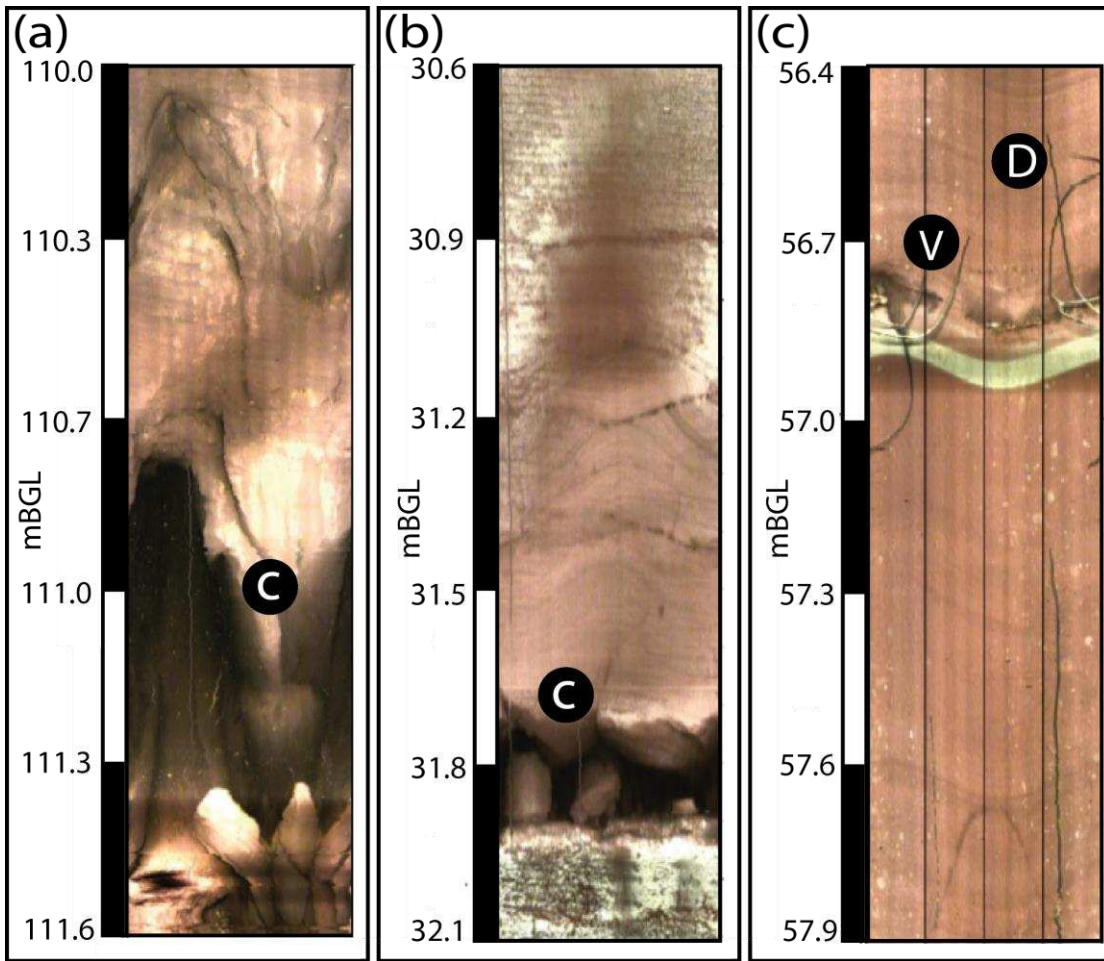
959



960

961 **Fig. 5** Outcropping fluvial (LA1) and aeolian (LA2) lithofacies association in the Sherwood  
 962 Sandstone Group. (a) Aeolian deposits Helsby Sandstone Formation, South Thurstaston,  
 963 Wirral Peninsula, (b) Aeolian deposits Helsby Sandstone Formation, North Thurstaston,  
 964 Wirral Peninsula, (c) Large cavity in fault zone, fluvial deposits of the St Bees Sandstone  
 965 Formation at St Bees, west Cumbria.

966



967

968 **Fig. 6** Fluvial deposits of the St Bees Sandstone Formation, optical logs in the St Bees-  
 969 Egremont area (west Cumbria, UK) from Medici et al. (2016). (a) Large cavity (C) in fault  
 970 zone, (b) cavity (C) in correspondence of a bedding plane discontinuity, (c) Dissolution (D)  
 971 of calcite veins (V).

972

973

974

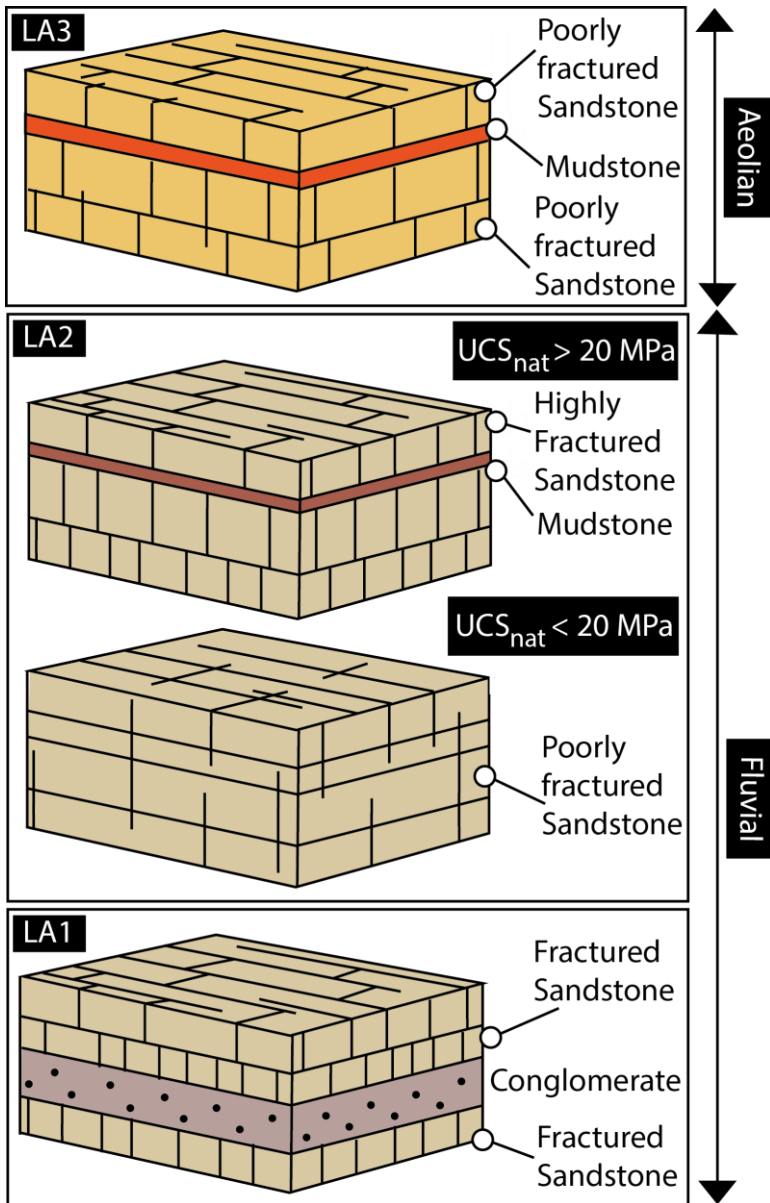
975

976

977

978

979



980

981 **Fig.7** Conceptual model of the fracturing network in the three lithofacies associations  
 982 (LA1-3) of the Sherwood Sandstone Aquifer (LA1 is fluvial conglomerate and pebbly  
 983 sandstone, LS2 sandstone channels interbedded with floodplain mudstone, LA3 cross-  
 984 bedded dune deposits of aeolian origin).

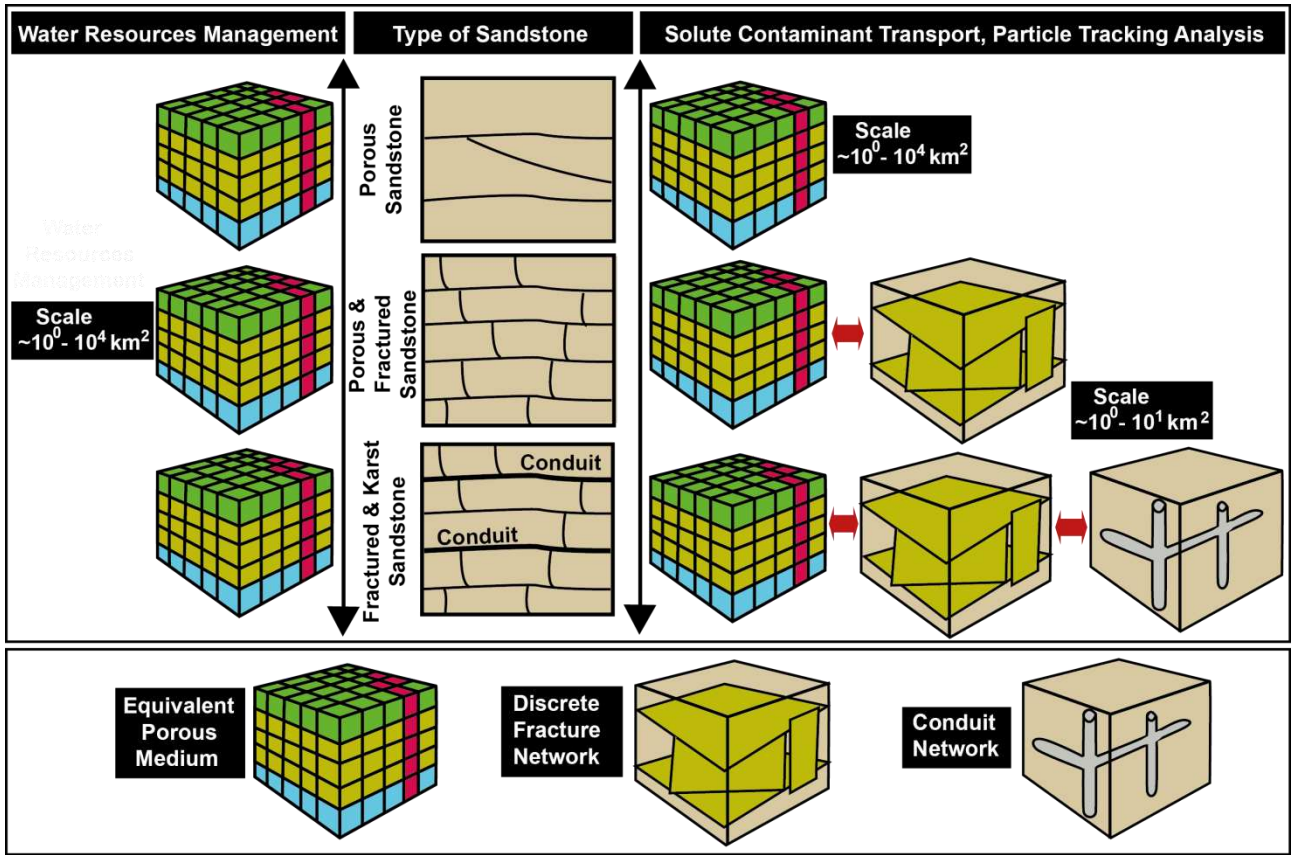
985

986

987

988

989



990

991 **Fig. 8** Selection of difference and finite elements modelling approaches (EPM, DFN and  
 992 CN) in sandstone aquifers as function of the permeability-type, observation scale and  
 993 modelling purpose.

994

995

996

997

998

999

1000

1001

1002

1003

1004

Numerical code	Sedimentary basin	Modelling objective	Reference
Equivalent Porous Medium			
MODLOW, MODPATH	Eastern England Shelf	Water balance, capture zone definition	Bottrell et al. 2006
			Zheng and Hiscock 2010
MODFLOW		Water balance	Bishop and Ruston 1993
			Neumann and Hughes 2003
MODLOW, MT3DMS		Water balance, solute contaminant transport	Davison and Lerner 2010
			Zheng and Hiscock 2011
	Zheng and Hiscock 2016		
MODFLOW	Worcester Basin	Water balance	Knipe et al. 1993
MODFLOW, MODPATH		Capture zone definition	Rivett et al. 2012
MODFLOW	Cheshire Basin	Fault compartmentalization assessment	Seymour et al. 2006
Discrete Fracture Network Models			
NAPSAC	Cheshire Basin	REV definition	Hitchmough et al. 2007

1005 **Tab. 1.** Type of approach, sedimentary basins and numerical code used for used for the  
1006 groundwater flow, particle tracking models and solute contaminant transport models used  
1007 in the Sherwood Sandstone Aquifer.